THE JOURNAL OF BIOLOGICAL CHEMISTRY VOL. 288, NO. 23, pp. 16655–16670, June 7, 2013

Cubilin, a High Affinity Receptor for Fibroblast Growth Factor 8, Is Required for Cell Survival in the Developing Vertebrate Head*[S]

Received for publication, January 14, 2013, and in revised form, April 15, 2013 Published, JBC Papers in Press, April 16, 2013, DOI 10.1074/jbc.M113.451070

Olivier Cases[‡], Aitana Perea-Gomez[§], Diego P. Aguiar[¶1], Anders Nykjaer[‖], Sabine Amsellem[‡], Jacqueline Chandellier[‡], Muriel Umbhauer[**], Silvia Cereghini[**], Mette Madsen[‡‡], Jérôme Collignon[§], Pierre Verroust[‡], Jean-François Riou[**], Sophie E. Creuzet[¶], and Renata Kozyraki[‡2]

*From the [‡]Institut de la Vision, INSERM U968, CNRS UMR7210, Université Pierre et Marie Curie UMRS968, 17 Rue Moreau, F-75012 Paris, France, the [§]Institut Jacques Monod, CNRS UMR7592, Université Paris Diderot, Sorbonne Paris Cité, 15 Rue Hélène Brion, F-75205 Paris, France, the [¶]Institut de Neurobiologie Alfred-Fessard, CNRS UPR3294, Développement, Evolution et Plasticité du Système Nerveux, F-91198 Gif-sur-Yvette, France, [‖]The Lundbeck Foundation Research Centre MIND, Department of Biomedicine, University of Aarhus, Olle Worms Allé 3, 8000 Aarhus, Denmark, **CNRS UMR7622, Laboratoire de Biologie du Développement, Université Pierre et Marie Curie, 9 Quai Saint Bernard, F-75252 Paris, France, and the [‡‡]Department of Biomedicine, University of Aarhus, Olle Worms Allé 3, 8000 Aarhus, Denmark*

Background: Cubilin is a multiligand endocytic receptor necessary for early embryonic development.
Results: Cubilin expressed in the developing head, namely the cephalic neural crest, binds Fgf8 and is required for cell survival and head morphogenesis.
Conclusion: Cubilin, Fgf8, and FgfRs act synergistically to promote anterior cell survival.
Significance: Cubilin is a novel modulator of the Fgf8-FgfR signaling activity.

Cubilin (Cubn) is a multiligand endocytic receptor critical for the intestinal absorption of vitamin B12 and renal protein reabsorption. During mouse development, Cubn is expressed in both embryonic and extra-embryonic tissues, and *Cubn* gene inactivation results in early embryo lethality most likely due to the impairment of the function of extra-embryonic *Cubn*. Here, we focus on the developmental role of *Cubn* expressed in the embryonic head. We report that Cubn is a novel, interspecies-conserved Fgf receptor. Epiblast-specific inactivation of *Cubn* in the mouse embryo as well as *Cubn* silencing in the anterior head of frog or the cephalic neural crest of chick embryos show that *Cubn* is required during early somite stages to convey survival signals in the developing vertebrate head. Surface plasmon resonance analysis reveals that fibroblast growth factor 8 (Fgf8), a key mediator of cell survival, migration, proliferation, and patterning in the developing head, is a high affinity ligand for Cubn. Cell uptake studies show that binding to Cubn is necessary for the phosphorylation of the Fgf signaling mediators MAPK and Smad1. Although Cubn may not form stable ternary complexes with Fgf receptors (FgfRs), it acts together with and/or is necessary for optimal FgfR activity. We propose that plasma membrane binding of Fgf8, and most likely of the Fgf8 family members Fgf17 and Fgf18, to Cubn improves Fgf ligand endocytosis and availability to FgfRs, thus modulating Fgf signaling activity.

Cubn encodes a 460-kDa peripheral membrane protein composed of eight epidermal growth factor repeats and 27 CUB domains (complement C1r/C1s, urchin Egf, bone morphogenic protein-1), which carry multiple potential sites for interaction with proteins, sugars, and phospholipids (1). Cubn is the physiological receptor for intrinsic factor-vitamin B12 in the gut and for albumin in the kidney (2). Distinct sets of mutations in *CUBN* either result in the Imerslund-Gräsbeck syndrome characterized by megaloblastic anemia and proteinuria (3) or in albuminuria and most likely end-stage kidney disease (4). Recently identified novel genetic polymorphisms in *CUBN* were evaluated as risk factors for neural tube defects (5, 6). It remains to be defined whether defects of this type are associated with the known Cubn implication in vitamin B12 homeostasis or with a novel developmental role of Cubn.

During mouse embryonic development, *Cubn* is expressed in various embryonic tissues as well as in the extra-embryonic visceral endoderm (7). *Cubn* gene deletion perturbs the formation of both embryonic and extra-embryonic derivatives, including somites and blood vessels, and leads to embryo lethality (8). Because extra-embryonic Cubn is critical for endocytosis of various maternally derived nutrients, including high density lipoproteins, a source of cholesterol (9, 10), the mouse knock-out phenotype was essentially attributed to nutrient deficiency resulting from a deficient maternal to fetal transport (8).

A recurrent difficulty when studying Cubn is to conciliate its endocytic function with its structure. Cubn lacks a trans-membrane domain (11). The internalization of Cubn-ligand complexes absolutely depends on the co-expression of additional proteins. We and others previously identified the trans-membrane proteins Lrp2 and Amn as endocytic partners for Cubn in the gut, kidney, and extra-embryonic visceral endoderm (11–

* This work was supported in part by INSERM, CNRS, UPMC, EuReGene FP6 Grant GA5085; CNRS-ANR-BLAN-0153, CNRS-ANR-06-BLAN-0200, the GEFLUC-Paris Ile de France; the Novo Nordisk Foundation, and the Lundbeck Foundation.
[S] This article contains supplemental Figs. 1–8.
[1] Recipient of a fellowship from Fondation des Treilles.
[2] To whom correspondence should be addressed. E-mail: renata.kozyraki@inserm.fr.

13). Lrp2 is the only currently known Cubn partner also to be expressed along with Cubn in the early embryo (7). In this context, it is interesting to note that lack of embryonic *Lrp2* perturbs forebrain development (14, 15) and that in *Lrp2* null mutants the internalization of Cubn ligands is decreased (2, 16).

In this study, we focus on the role of embryonic Cubn during the early steps of anterior head formation. We show that *Cubn* is expressed in the anterior cephalic mesenchyme, cephalic neural crest cells (CNCCs),[3] and forebrain neuroepithelium and that it is critical for cell survival and rostral head morphogenesis in the mouse, frog, and chick embryos. We provide *in vivo* evidence that Cubn acts synergistically with Fgf8, a morphogen essential for CNCC survival, migration, and proliferation and for telencephalic patterning. We identify Fgf8 as a novel Cubn ligand and show that Cubn is necessary for Fgf8-dependent phosphorylation of the Fgf targets MAPK/ERK *in vitro*. Furthermore, we provide evidence that Cubn and the Fgf8 receptor FgfR3 functionally interact in the developing head.

EXPERIMENTAL PROCEDURES

Mice—Animal procedures were conducted in strict compliance with approved institutional protocols and in accordance with the provisions for animal care and use described in the European Communities Council Directive of 24 November 1986 (86/609/EEC). *Sox2*.Cre (B6.Cg-Tg (Sox2-cre) 1AmcJ) and *Foxg1*.Cre (129.Cg-*Foxg1*$^{tm1(cre)Skm}$/J) were purchased from The Jackson Laboratory (Bar Harbor, ME). *Cubn*$^{Lox/Lox}$ mice (supplemental Fig. 1, *A* and *B*) have been described previously (2). The midnight before the morning with a copulation plug was considered as embryonic day 0 (E0.0). A small fragment of embryos or a piece of yolk sac was used for genotyping according to standard procedures. The absence of residual Cubn expression was confirmed by Western blotting using various monoclonal and polyclonal anti-Cubn antibodies that detect all Cubn extracellular modules, *i.e.* both EGF and CUB domain regions (supplemental Fig. 1*C*).

In Situ RNA Hybridization—Heart-beating embryos were fixed and analyzed by whole-mount *in situ* RNA hybridization according to standard procedures.

Simultaneous Detection of Cell Death and Proliferation—Lysotracker Red (Invitrogen, DND99) staining was described previously (17). For cell proliferation, anti-phospho-histone H3 (1:250, Millipore, Molsheim, France) followed by Alexa 488-conjugated goat anti-rabbit (1:200, Invitrogen) was used. Nuclear staining was achieved by a 20-min incubation in Hoechst 33342 (Invitrogen). Images were collected by confocal microscopy (LSM710 ConfoCor 3, Carl Zeiss) and processed using ImageJ software. Total numbers of Lysotracker- and pH 3-positive profiles were counted in 15 and 23 consecutive sections for E8.75 and E9.25 embryos, respectively; in some cases four consecutive medial or more superficial sections were used.

Immunocytochemistry and Vital Staining—Fixed whole embryos or frozen sections (10 μm thick) were processed for immunocytochemistry using rabbit anti-Cubn (1:1,000), sheep anti-Lrp2 (1:4,000), rat anti-PECAM1 (1:75; Pharmingen), or rabbit-anti-Tfap2a (1:100; Santa Cruz Biotechnology) antibodies. In some cases frozen sections were counterstained with Nissl (Sigma).

Protein Analysis—Embryos and subconfluent cells were lysed in a PBS buffer containing 10 mM NaH_2PO_4, 150 mM NaCl, 6 mM $CaCl_2$, 1% Triton X-100, 1 mM Na_3VO_4 (Sigma), and Complete mini EDTA-free protease inhibitor mixture tablets (Roche Diagnostics), 2 mM sodium orthovanadate, and phosphatase inhibitor mixture 1 (Sigma).

For Western blot analysis, 10 μg of total protein was applied to each well. Equal loading was verified by blotting for GAPDH. Primary antibodies used were as follows: rabbit anti-P-Akt (Ser-473; 1:1,000; Cell Signaling); total anti-Akt (1:1,000; Cell Signaling); goat anti-BMP7 (1:3,000; Abcam); goat anti-β-catenin (1:500; Santa Cruz Biotechnology, C-18); mouse anti-P-β-catenin (1:500; Santa Cruz Biotechnology, 1B11); rabbit anti-cleaved caspase 3 (1:2,500; Cell Signaling, 9661); goat anti-chordin (1:500; Santa Cruz Biotechnology, V-18); mouse anti-Cubn (1:4,000) (18); rabbit anti-Cubn (1:5,000); rabbit anti-P-Erk1/2 (Thr-202/204; 1:1,000; Cell Signaling); rabbit anti-Erk1/2 (1:1,000; Cell Signaling); mouse anti-Fgf2 (1:500, Santa Cruz Biotechnology); mouse anti-Fgf3 (1:500; Santa Cruz Biotechnology, MSD1); goat anti-Fgf8b (1:1,000; AF423-NA, R&D Systems); mouse anti-Fgf8b (1:1,000; MAB323, R&D Systems); rabbit anti-Fgf8 (1:500, 7916, Santa Cruz Biotechnology); goat anti-Fgf15 (1:500; Santa Cruz Biotechnology, P-20); mouse anti-Fgf17 (1:500, Santa Cruz Biotechnology, B-4) and goat anti-Fgf17 (1:500, Santa Cruz Biotechnology, C-14); rabbit anti-FgfR1 (1:1000; 52153, Abcam); rat anti-FgfR2c (1:1,000; MAB716, R&D Systems); mouse anti-FgfR3c (1:1,000; MAB7662, R&D Systems); rabbit anti-Noggin (1:500; Santa Cruz Biotechnology, Fl-232); rabbit anti-PSmad1 (Ser-206; 1:1,000; Cell Signaling); rabbit anti-Smad1 (1:1,000; Cell Signaling); rabbit anti-PSmad1/5/8 (1:1,000; Pharmingen); rabbit anti-Wnt1 (1:500; Santa Cruz Biotechnology, H-89); rabbit anti-Wnt3 (1:500; Santa Cruz Biotechnology, H-70); and goat anti-Wnt8b (1:500; Santa Cruz Biotechnology, 25177).

Morpholino Oligonucleotide Design and Injection in Xenopus laevis Eggs—Embryos were obtained as described previously (19). A 122-bp sequence was amplified from St.36 cDNA using primers corresponding to the first exon of *X. tropicalis Cubn* gene model (5′-AGACTCACAGCTGGAGGGAA-3′; 5′-TCTCCAGACTCGCACATCAG-3′) and was further expanded using 5′rapid amplification of cDNA ends-PCR (Smarter RACE cDNA amplification kit, Clontech–Takara). The 5′ region of *X. laevis Cubn* mRNA was cloned to design two translation-blocking morpholinos. Specific morpholino targeting the start codon (MoCubn, 5′-AAGGTAGGAAGCCTCGGGAAAGCAT-3′) or the 5′UTR (Mo1Cubn, 5′-CCCCATGTACTCTGCGTTGATACCA-3′) was used (Gene Tools, Philomath, OR). MoFgf8 (5′-GGAGGTGATGTAGTTCATGTTGCTC-3′) targeting *Fgf8* as well as an unrelated control morpholino (5′-TCGTCCACTTGTTCGCTCAATCGAT-3′) were previously described. Morpholinos, at doses ranging from 2.5 to 10 pmol, were microinjected into the two blastomeres at the 2-cell stage for protein analysis. For

[3] The abbreviations used are: CNCC, cephalic neural crest cell; FgfR, Fgf receptor; nt, nucleotide; ss, somite stage; BN/MSV, brown Norway rat/mouse sarcoma virus; SPR, surface plasmon resonance; ANR, anterior neural ridge; CE, cephalic ectoderm.

anterior developmental analysis, the morpholinos were injected at the 8-cell stage. To target knockdown to the anterior left side of the head and to control proper targeting, doses varying from 0.125 to 1 pmol were injected into the left dorso/animal blastomere together with 5 ng/nl rhodamine-lysinated dextran (Invitrogen) as lineage tracer. The right side was used as a control. Standard procedures were used for *in situ* RNA hybridization.

RT-Quantitative PCR—X. laevis Cubn primers sequences were chosen in the 3′ end of the mRNA as follows: forward, 5′-GAGACGACAAGTTCATCTTCATGC-3′ (nts 183); reverse, 5′-CCGAGTCACTGCCATTTCTCA-3′ (nts 243). Cytoskeletal actin was used as reference gene as follows: forward, 5′-TCTATTGTGGGTCGCCCAAG-3′ (nts 158); reverse, 5′-TTGTCCCATTCCAACCATGAC-3′ (nts 208). Quantification of *X. lævis Cubn* mRNA expression was carried out at late neurula stage (st. 20). The anterior neural plate was dissected out. The embryo was further dissected into truncal and caudal halves. Batches of six explants were processed for RNA extraction using the RNeasy kit (Qiagen SA). One μg of total RNA was used for reverse transcription (Applied Biosystems, Carlsbad, CA). Quantitative RT-PCR was performed using Fast SYBR Green Master Mix (Applied Biosystems).

Cell Culture—Brown Norway rat yolk sac epithelial cells transformed with mouse sarcoma virus (BN/MSV) were grown as described previously (18). BN/MSV cells were seeded in 24-well plates and used at subconfluence. Overnight serum-starved cells were incubated for 5 min with 5 ng/ml Fgf8b (catalog no. 423-F8, R&D Systems) or 5 ng/ml heparin-stabilized FGF2 (F9786; Sigma). Recombinant Cubn fragments expressing CHO cells were previously described (20).

SPR Analysis, Immunoprecipitation—SPR analysis was performed on a Biacore 3000 as described previously (21). Cubilin was immobilized (at 10^{-15} g ml^{-1}) on a CM5 chip, and the remaining coupling sites were blocked with 1 M ethanolamine. The sample and running buffer was 10 mM HEPES, 150 mM $(NH_4)_2SO_4$, 1.5 mM $CaCl_2$, 1 mM EGTA, 0.005% Tween 20, pH 7.4 (all products from Sigma). Recombinant mouse FGF8b and Fgf8a (catalog nos. 423-F8 and 4745-F8, R&D Systems) were applied in increasing concentration, and the sensor chip regenerated in a 10 mM glycine-HCl buffer after each analytic cycle. The SPR signal was expressed in relative response units as the response obtained in a control flow channel was subtracted. Recombinant FgfR1 (catalog nos. 658 and 655, R&D Systems) and FgfR2 (catalog nos. 665, 716, R&D Systems) were used. Mouse Cubn was purified by affinity chromatography of renal extracts on an intrinsic factor-vitamin B12 column as described previously.

Immunoprecipitation—Cephalic extracts of E8.75–9.0 embryos or cell lysates of conditioned CHO media were applied on Sepharose A or Sepharose G (GE Healthcare) beads coupled with anti-Cubn, anti-Fgf8b, or anti-Fgf17 antibodies. Immunoprecipitation was performed using standard procedures. Control immunoprecipitation was performed with rabbit or mouse preimmune serum. All precipitated proteins were analyzed by reducing SDS-PAGE and were detected by autoradiography using ECL reagents as described by the manufacturer (GE Healthcare).

Functional Assays in Avian Embryos— dsRNA were synthesized from cDNA encoding for the following targeted genes: *dsCubn1* (nts 581–883, exons 7–8); *dsCubn2* (nts 6680–7034, exons 44–45); *dsFgfR1* (nts 605–891, exons 5–7); *dsFgfR2* (nts 785–1106, exons 5–6); *dsFgfR3* (nts 612–927, exons 6–7). *In ovo* electroporation was performed as described previously (22). Briefly, electroporation in the developing head was performed in chick embryos at 5–6 somites stage (5–6 ss, *i.e.* 30 h of incubation at 37 °C). Exogenous nucleic sequences *dsCubn, dsFgfR1, dsFgfR2,* and *dsFgfR3* or combinations (200 ng/μl) and RCAS-*Noggin* were mixed in a solution of Fast Green FCF (0.01%, Sigma), bilaterally transfected to the cephalic NC cells or transfected to the cephalic NC cells and cephalic ectoderm. For control series, nonannealed sense and antisense RNA strands corresponding to the sequences of the targeted genes were transfected at the same concentrations. The efficiency of the silencing was confirmed by *in situ* hybridization analysis. For protein supplementation, heparin-acrylic beads (Sigma) soaked with a solution of Fgf8b recombinant protein (5 μM; R&D Systems) were used.

Statistical Analysis and Graph Plotting—SigmaStat (Systat Software Inc., Richmond, CA) was used for data analysis. Excel (Microsoft) was used to plot data.

RESULTS

Cubn Is Expressed in the Cephalic Neuroepithelium and Neural Crest Cells during Early Somite Stages—In pre-somitic stages, Cubn mRNA is strongly expressed in the extraembryonic visceral endoderm (Fig. 1, *A–C*) (7). During neurulation (E8.5, 5–7 ss) Cubn mRNA is found in the prospective forebrain neuroepithelium, the optic eminences, and the cephalic mesenchyme (Fig. 1, *D* and *E*). Cubn immunostaining reveals that Cubn is distributed at the apical pole (7) of the neuroepithelial cells (Fig. 1, *F–H* and *J*) as well as along the plasma membrane of cells adjacent to the cephalic neural folds and the surface ectoderm (Fig. 1, *G* and *I–L*). At E9.0 (13–16 ss) Cubn mRNA and protein are readily detected in the ventral forebrain and pharyngeal regions and at low levels in the mesenchyme of the dorsal forebrain, mid-, and hindbrain (Fig. 1, *M* and *N*). Double immunostaining for Cubn and the neural crest marker Tfap2α shows that Cubn is partly expressed in Tfap2α-positive CNCCs (Fig. 1, *N–P*). In these cells, Cubn is also co-expressed with Lrp2 (Fig. 1, *Q–S*).

Sox2-Cre-mediated Ablation of Embryonic Cubn Leads to Rostral Head Hypoplasia by E9.5—To inactivate embryonic *Cubn*, we used a floxed *Cubn* allele (supplemental Fig. 1, *A* and *B*) and the *Sox2-Cre* transgene. Whereas the maternally inherited transgene recapitulates the null phenotype (supplemental Fig. 1, *C–M*), as reported previously (8), the paternally inherited *Sox2-Cre* transgene that we used here induces recombination only in epiblast cells from E6.5 onward (24) and leads to inactivation of Cubn in both the neuroepithelium and the mesenchyme (supplemental Fig. 1, *N–S*). CubnL/+;Sox2-Cre heterozygous mice were viable and morphologically normal. CubnL/L; Sox2-Cre (hereafter designated as $Cubn^{sox2\text{-}cre\text{-}KO}$) mutants did not develop beyond E12.5 (Table 1). At E8.5 (Fig. 2, *A* and *A′*), the morphology of the $Cubn^{sox2\text{-}cre\text{-}KO}$ mutants was similar to that of the controls. From E9.5 (~25 ss) onward and

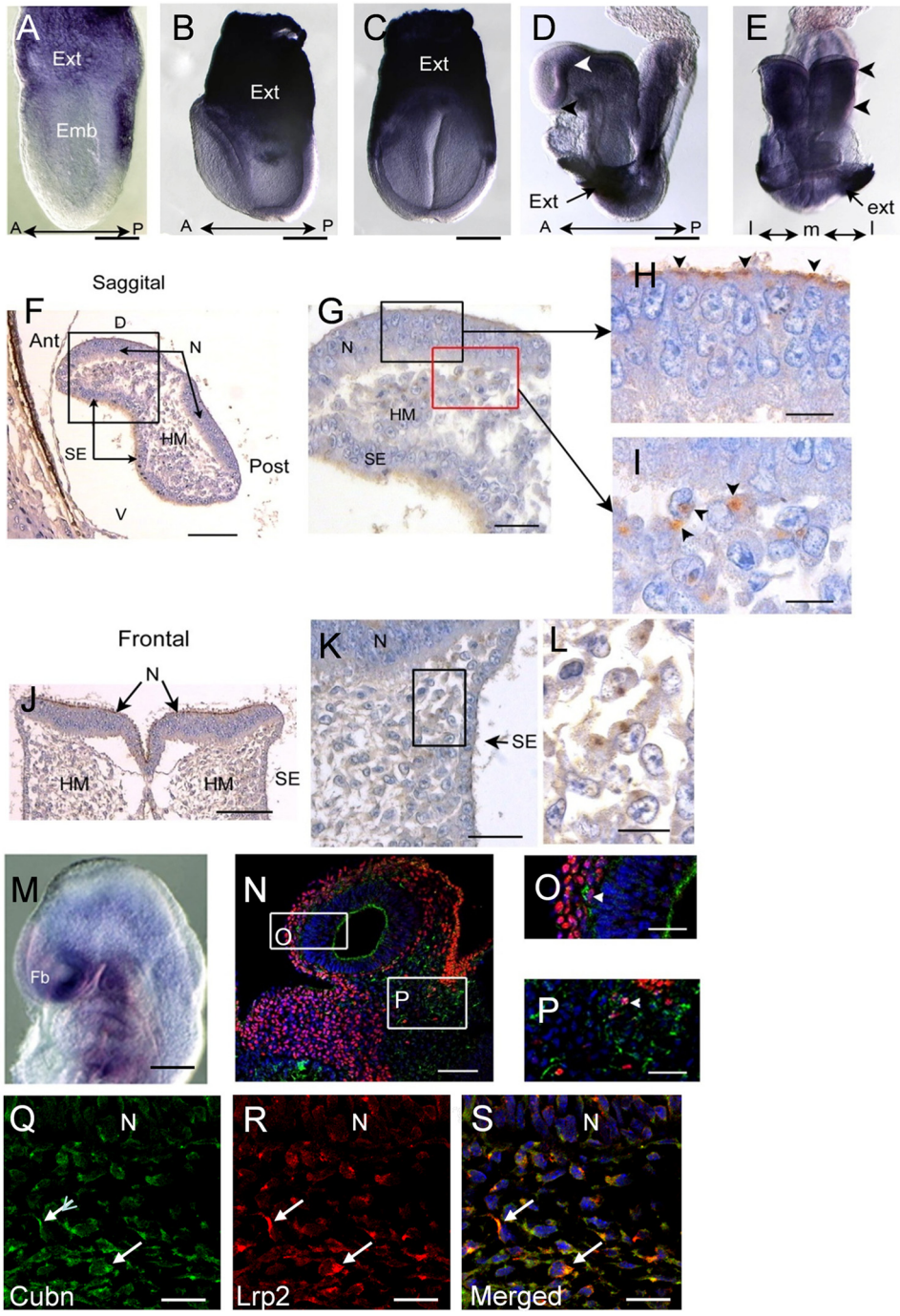

FIGURE 1. **Cubn distribution in the early mouse embryo.** *A–C,* strong *Cubn* mRNA expression in the extra-embryonic (*Ext*) tissues during gastrulation (*A,* lateral view) and early headfold stages (*B* and *C*, lateral and frontal views). *D–L, Cubn* mRNA and protein expression at E8.5; *Cubn* is found in the forebrain (*white arrowhead* in *D*, lateral view) and the cephalic mesenchyme (*arrowheads* in *E*, frontal view); *black arrowhead* in *D* points to the ANR. *F–L,* sagittal (*F–I*) and frontal (*J–L*) paraffin sections through the forebrain show Cubn distribution at the apical pole of neuroepithelial cells (*arrowheads* in *H*) and at the plasma membrane of mesenchymal cells (*arrowheads* in *I*). *M, Cubn* mRNA (lateral view) in the forebrain (*Fb*), the cephalic mesenchyme of the fore-, mid-, and hindbrain regions, and the pharyngeal region at E9.0. *N–P,* sagittal cryosection of an E9.0 embryo shows partial co-localization of Cubn (*green*) and Tfap2α (*red*) in the migratory neural crest at the level of the forebrain (*O*) and midbrain (*P*) mesenchyme. Cubn is also detected in the forebrain (*N* and *O*). *Q–S*, Cubn (in *green*) and Lrp2 (in *red*) co-localize in the migratory neural crest of the same embryo (*arrows*). *A,* anterior; *P,* posterior; *D,* dorsal; *V,* ventral; *m,* medial; *l,* lateral; *emb,* embryonic; *hm,* head mesenchyme; *N,* neuroepithelium; *se,* surface ectoderm. *Scale bars, A,* 175 μm; *B* and *C,* 200 μm; *D* and *E,* 250 μm; *F* and *J,* 125 μm; *G* and *K,* 80 μm; *H, I,* and *L,* 50 μm; *M,* 250 μm; *N,* 175 μm; *O* and *P,* 75 μm; *Q–S,* 15 μm.

despite the apparently normal body axis and heart formation, the forebrain, in particular the telencephalon, was markedly reduced in size (33% compared with the controls, $n = 7$), and the optic vesicles were hypoplastic or absent (Fig. 2, *B–F′*). Despite the reduction, the general prosomeric organization of the mutant forebrain was preserved until E10.5 (Fig. 2, *D* and *D′*).

To find out whether *Cubn* is necessary in the early forebrain neuroepithelium, we used the *Foxg1-Cre* allele widely expressed in the forebrain and the facial ectoderm around E9.0

TABLE 1
Embryonic lethality of *Cubn*$^{Sox2\text{-}cre\text{-}KO}$ mutants

	Cubn$^{L/L}$ × Cubn$^{L/+}$;*Sox2-Cre* intercross			
	Cubn$^{L/+}$, *Cubn*$^{L/L}$	*Cubn*$^{LL/+}$;*Sox-Cre*	*Cubn*$^{L/L}$;*Sox2-Cre*	Total
E9.5	206 (58%)	78 (22%)	69 (20%)	353
E12.5	41 (73%) 50%	15 (27%) 25%	0 25%	56

(25). Despite *Cubn* deletion, residual Cubn immunostaining was still detectable in the telencephalon of E10.5 *CubnL/L*; *Foxg1-Cre* mutants. Telencephalic development was normal in these mutants, and only minor cortical defects, including the absence of corpus callosum, could be evidenced at later stages (supplemental Fig. 2). We therefore focused on the *Cubn*$^{Sox2\text{-}Cre\text{-}KO}$ mutants.

Forebrain and Face Hypoplasia in E9.25 Cubn$^{Sox2\text{-}Cre\text{-}KO}$ *Mutants Correlates with Decreased Cell Survival*—At E9.25 (~20 ss), prior to the appearance of major telencephalic hypoplasia, cell proliferation evidenced by the M-phase cell cycle marker phospho-histone H3 (PH3) was not modified in the cephalic region of *Cubn*$^{Sox2\text{-}Cre\text{-}KO}$ mutants (Fig. 3, *A*, *A′*, and *B,* and supplemental Fig. 3, *A* and *B′*). However, cell death, followed by the fluorescent dye Lysotracker (26), was significantly increased in the anterior mutant head (Fig. 3, *A*, *A′*, and *C*), both in the ventral and dorsal cephalic mesenchyme (supplemental Fig. 3, *A* and *A′*). At this stage, Lysotracker staining was marginal in the telencephalic neuroepithelium (supplemental Fig. 3, *B* and *B′*). Immunoblotting of E9.25 anterior cephalic extracts showed increased expression of activated caspase-3 in the mutants (supplemental Fig. 3*C*), indicating enhanced apoptosis.

Forebrain Patterning Is Maintained in E9.25 Cubn$^{Sox2\text{-}Cre\text{-}KO}$ *Mutants*—We next performed a detailed molecular analysis of the forebrain. Regional specification of the forebrain is controlled by at least three signaling centers that work synergistically and regulate each other (27–30). The rostral patterning center expresses Fgfs, including *Fgf8,* and controls the size and ventral patterning of the forebrain. The dorsal patterning center expresses Bmps and Wnts and is involved in the development of dorsal-caudal structures; the ventral patterning center expresses *Shh.* If *Shh* is lost, Bmp activity and Bmp-responsive genes are up-regulated, and *Fgf8* expression is lost. Furthermore, excess of Bmps down-regulates both *Fgf8* and *Shh*.

Foxg1, Fgf8, and *Fgf17* were normally distributed in the anterior telencephalon of ~E9.25 *Cubn*$^{Sox2\text{-}Cre\text{-}KO}$ mutants (Fig. 3, *D–F′*). The occupancy percentage of *Foxg1* in the telencephalon was identical in the mutants and wild-type littermates (35% *versus* 33%, respectively, $n = 4$) indicating that the reduction of the *Foxg1* expression domain was due to the hypoplasia of the forebrain. Similarly, the expression domain of *Six3* was reduced in the mutant hypoplastic rostroventral telencephalon and optic vesicles (Fig. 3, *G* and *G′*). *Shh* was absent from the mutant preoptic area only (Fig. 3, *H* and *H′*), and *Nkx2.1,* which is necessary in the ventral forebrain for the activation of *Shh*, was also absent from the preoptic area but remained normal in the hypothalamus (Fig. 3, *I* and *I′*). *Spry1*, an Fgf signaling antagonist, was present in the mutant commissural plate and isthmus but did not expand ventrally in the ventral cephalic ectoderm (supplemental Fig. 3, *D* and *D′*). *Emx2* along the dorsal telencephalon (Fig. 3, *J* and *J′*) and *Bmp7* at the dorsal midline were similarly expressed in the wild-type and mutant embryos (supplemental Fig. 3, *E* and *E′*). Finally, the diencephalic marker *Wnt8b* was normally expressed in the mutants, and *En2* was normally detected at the diencephalic-mesencephalic boundary (supplemental Fig. 3, *F* and *G′*). The above data show that, despite the strong reduction of the forebrain tissue and the discrete patterning defects, forebrain organization is maintained in the *Cubn*$^{Sox2\text{-}Cre\text{-}KO}$ mutants.

Abnormal Distribution of CNCCs Contributes to Head Defects in Cubn$^{Sox2\text{-}Cre\text{-}KO}$ *Mutants*—CNCC is a migratory population that derives from the dorsal fore-, mid-, and hindbrain and contributes to head morphogenesis. The survival, migration, and patterning of CNCCs require signals of the previously cited patterning centers (31–33).

The rostroventral expression of the CNCC markers *Tfap2α* and *Dlx2* was patchy at the level of the mutant telencephalon and in the periocular region. These markers were normally expressed in the first brachial arch (Fig. 3, *K–L′*). The ectodermal and CNCC marker *Dlx5* was decreased rostrally at the level of the mutant telencephalic region but remained expressed in the ventral most cephalic ectoderm and brachial arch region (Fig. 3, *M* and *M′*). Thus, around E9.25, a stage at which in wild-type embryos the spread of the CNCC over the forebrain and first brachial arch region is complete, the distribution of representative CNCC markers is abnormal in the mutants suggesting that defective migration and/or survival of the CNCC in the rostral head contributes to the cephalic hypoplasia in the *Cubn*$^{Sox2\text{-}Cre\text{-}KO}$ mutant embryos.

Normal Forebrain Regionalization and Perturbed Fgf Signaling in E8.75 Cubn$^{Sox2\text{-}Cre\text{-}KO}$ *Mutants*—To identify the onset of the defects, we analyzed mutant embryos at earlier developmental stages. We could not see any alteration in the expression of the early anterior neuroectoderm and rostrolateral ectoderm markers Otx2, Dlx5, Hesx1, and Six3 (supplemental Fig. 4, *A–D′*) between E7.5 and E8.25, and Fgf8 was normally induced at the mutant anterior neural ridge (ANR), prospective rostral patterning center, at E8.25 (supplemental Fig. 4, *E* and *E′*) indicating that forebrain specification was normally initiated in the mutants.

At E8.75 (8–10 ss) the *Cubn*$^{Sox2\text{-}Cre\text{-}KO}$ mutants were phenotypically normal. The rates of cell proliferation and cell death were similar in the forebrain and surrounding tissues of E8.75 mutant and wild-type littermates (Fig. 4, *A* and *A′* and supplemental Fig. 5, *A* and *B*). *Fgf8* was maintained in the mutant ANR (Fig. 4, *B* and *B′*) and *Foxg1* expression similarly marked the mutant ANR and neuroectoderm (Fig. 4, *C* and *C′* and supplemental Fig. 5, *C–D′*). The expression of the BMP antagonist-encoding *Noggin* and of *Bmp7* was unaffected in the mutant axial mesendoderm (Fig. 4, *D* and *D′* and supplemental Fig. 5, *E* and *E′*). *Bmp4* was not ectopically expressed in the mutants (supplemental Fig. 5, *F* and *F′*). *Wnt1* and *Wnt8b* were normally distributed in the presumptive diencephalon and midbrain (Fig. 4, *E–F′*). *Shh* was unaffected in the mutant neuroectoderm and axial mesendoderm (supplemental Fig. 5, *G* and *G′*), and *Gli1*, whose transcription is absolutely dependent on Shh signaling, was normally expressed in the mutant ventral forebrain

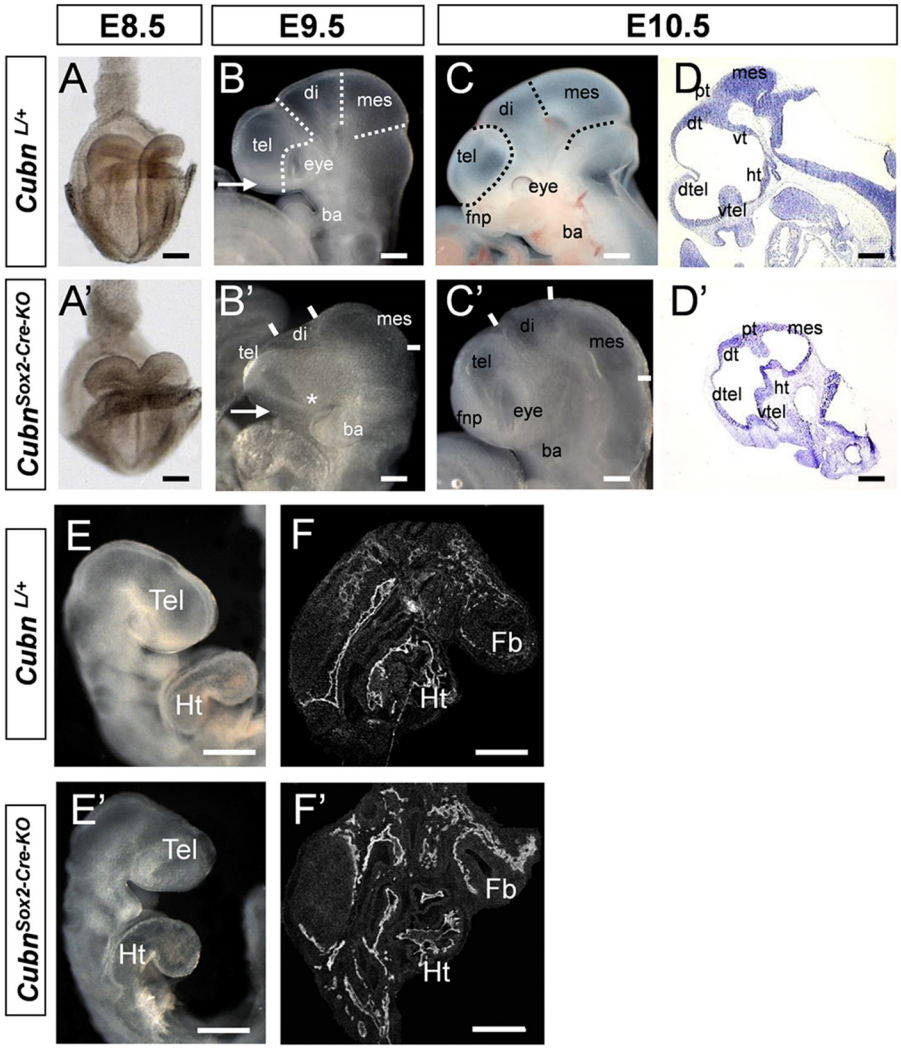

FIGURE 2. **Epiblast-specific inactivation of mouse *Cubn* impairs early head formation.** *A–F′*, morphology of $Cubn^{Sox2\text{-}Cre\text{-}KO}$ mutants and wild-type littermates between E8.5 and E10.5. *A* and *A′*, normal morphology at E8.5 (frontal view). *B–C′*, mutant telencephalon (*tel*), eye (*asterisk* in *B′*), and frontonasal process (*fnp, arrows* in *B* and *B′*) are reduced at E9.5 and 10.5 (lateral views). *D* and *D′*, sagittal cryosections showing a marked reduction of the mutant ventral (*vtel*) and dorsal telencephalon (*dtel*). *E* and *E′*, normal heart positioning and looping in the mutant at E9.5. *F* and *F′*, PECAM-1 immunostaining on sagittal cryosections through the forebrain and heart shows well developed blood vessels in both the mutant and control embryos. *Di,* diencephalons; *dt,* dorsal thalamus; *fb,* forebrain; *fp,* floorplate; *ht,* hypothalamus; *Ht,* heart; *mes,* mesencephalon; *vt,* ventral thalamus; *pt,* pretectum. *Scale bars, A,* 300 μm; *B–F,* 200 μm.

(supplemental Fig. 5, *H* and *H′*). *Six3*, a repressor of *Wnt1* and *Wnt8b* (34, 35) and an activator of *Shh,* appropriately marked the developing mutant ventral forebrain and eyes (supplemental Fig. 5, *I* and *I′*). Finally, the early CNCC and ectodermal markers *Tfap2α, Msx1*, *Dlx5,* and *Dlx2* were normally distributed at the dorsal neural folds of the mid- and hindbrain and in the cephalic ectoderm (Fig. 4, *G–H′* and supplemental Fig. 5, *J–K′*). *Noggin* was also normally detected along the dorsal neural folds and in the lateral cephalic mesenchyme of the mutants (Fig. 4, *I* and *I′*). Thus, overall forebrain regionalization and CNCC generation are normal in E8.75 $Cubn^{Sox2\text{-}Cre\text{-}KO}$ mutants.

MAPK/ERK Signaling Appears to be Deficient in E8.75 $Cubn^{Sox2\text{-}Cre\text{-}KO}$ Mutants—To understand why, despite normal neuroepithelial and neural crest marker expression at E8.75, increased apoptosis and perturbed CNCC distribution were evidenced half a day later in the mutants, we investigated whether the main signaling pathways involved in anterior cell survival, early forebrain regionalization, and global head morphogenesis were active (36–38). We analyzed the phosphorylation of the known Tgf-β/BMP, Wnt, and Fgf signaling effectors in anterior cephalic extracts of E8.75-E9.0 control and mutant embryos. Similar expression levels of phospho-Smad1/5/8 and phospho-Smad2 suggested that the intensity of Tgf-β/BMP activity was unaffected in the mutants (Fig. 4*J*). Wnt signaling-dependent GSK3 and Fgf/MAPK/ERK activities modulate the duration of the Bmp signal by catalyzing phosphorylation of Smad1 in the linker region, predominantly at Ser-206 (39, 40). We could not detect Smad1 phosphorylated at Ser-206 in the mutants (Fig. 4*J*). As suggested by the similar levels of β-catenin and phosphorylated β-catenin in control and mutant extracts (Fig. 4*J*), this was not due to modified Wnt and presumably GSK3 activity. We therefore analyzed the phosphorylation of ERK1/2 that mediates intracellular responses downstream to Fgf/FgfR signaling in the anterior head (41, 42) and triggers linker phosphorylation of Smad1 (39). The levels of ERK1/2 were clearly decreased in the mutant extracts (Fig. 4*K*) suggesting decreased Fgf activity. However,

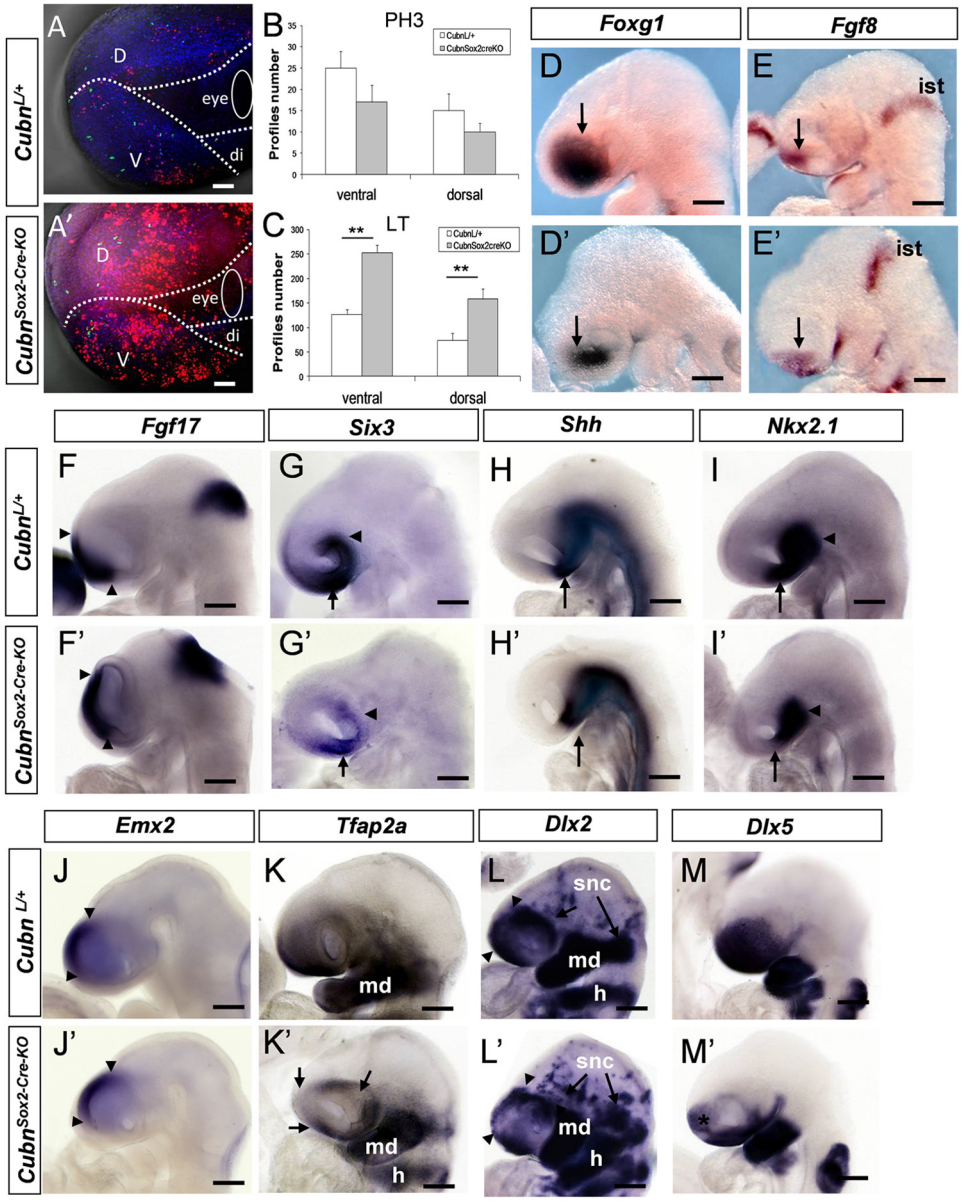

FIGURE 3. **Increased apoptosis and impaired expression of CNCC markers in the *Cubn*$^{Sox2\text{-}Cre\text{-}KO}$ mutant heads around E9.25.** *A* and *A′*, representative lateral views of control and *Cubn*$^{Sox2\text{-}Cre\text{-}KO}$ embryos stained with Lysotracker (in *red*) and anti-phospho-histone H3 (in *green*). *Dotted lines* demarcate the ventral cephalic region (*v*), dorsal cephalic region (*d*), and diencephalic region (*di*) of E9.25 control (*A*) and mutant (*A′*) embryos. *B* and *C*, cell proliferation is similar at E9.25 (*B*), whereas the number of Lysotracker+ (*LT*) cells (*C*) is significantly increased in the mutant forehead (mean ± S.E., $n = 3$ embryos of each genotype; Student's *t* test, $p < 0.05$). *D–M′*, representative whole-mount mRNA staining of control (*D–M*) and mutant (*D′–M′*) embryos around E9.25. *D* and *D′*, reduced expression domain of *Foxg1* in the mutant telencephalon (*arrows*). *E* and *E′*, *Fgf8* is normally expressed in the commissural plate (*arrow*) and the isthmus (*ist*). *F* and *F′*, *Fgf17* is normally detected at the commissural plate (*arrowheads*) and isthmus. *G* and *G′* reduced expression domain of *Six3* in the ventral telencephalon (*arrow*) and eye region (*arrowhead*). *H* and *H′*, *Shh* is lost in the mutant preoptic area (*arrow*). *I* and *I′*, down-regulation of *Nkx2.1* in the mutant preoptic area (*arrow*) but not the hypothalamus (*arrowhead*). *J* and *J′*, dorsal domain of *Emx2* is conserved (*arrowheads*). *K* and *K′*, *Tfap2a* displays a patchy distribution in the mutant telencephalon and periocular region (*arrows*). *L* and *L′*, patchy *Dlx2* expression in the mutant rostral cephalic tissues (*arrowheads*), and in migratory cephalic neural crest cells that contribute to the neurogenic sensory cranial ganglia (*snc*; *arrows*). *Dlx2* is normally expressed in the mandibular (*md*) component of the first branchial arch and in the hyoid (*h*). *M* and *M′*, down-regulation of *Dlx5* in the mutant rostro-ventral cephalic tissues (*asterisk*). Lateral views, anterior is to the *left*. *Scale bars, A,* 75 μm; *D–M,* 200 μm.

the unaltered levels of phospho-Akt, another Fgf effector in the anterior head (Fig. 4*K*), and of FgfR1–3 indicated that Fgf signaling was at least partly operating in the mutants, a finding consistent with the normal forebrain patterning. Taken together, these results support the idea that in E8.75–9.0 *Cubn*$^{Sox2\text{-}Cre\text{-}KO}$ mutants the pro-survival Fgf signals may be not efficient enough to limit the duration of the pro-apoptotic Bmp activity, eventually contributing to increased anterior cell death and head hypoplasia.

High Affinity Binding of Fgf8 to Cubn Leads to Efficient ERK1/2 and Smad1 Linker Phosphorylation—To understand how Cubn may affect the Fgf signaling pathway, we sought for potential interactions between Cubn and Fgf8, the best studied Fgf ligand during head morphogenesis. Fgf8 as well as the Fgf8 subfamily member, the structurally similar Fgf17 (43), were co-immunoprecipitated with Cubn in anterior cephalic extracts of wild-type E8.75–9.0 embryos (Fig. 5*A*). Structurally distinct Fgfs, including Fgf2 and the ANR-produced Fgf3 and Fgf15,

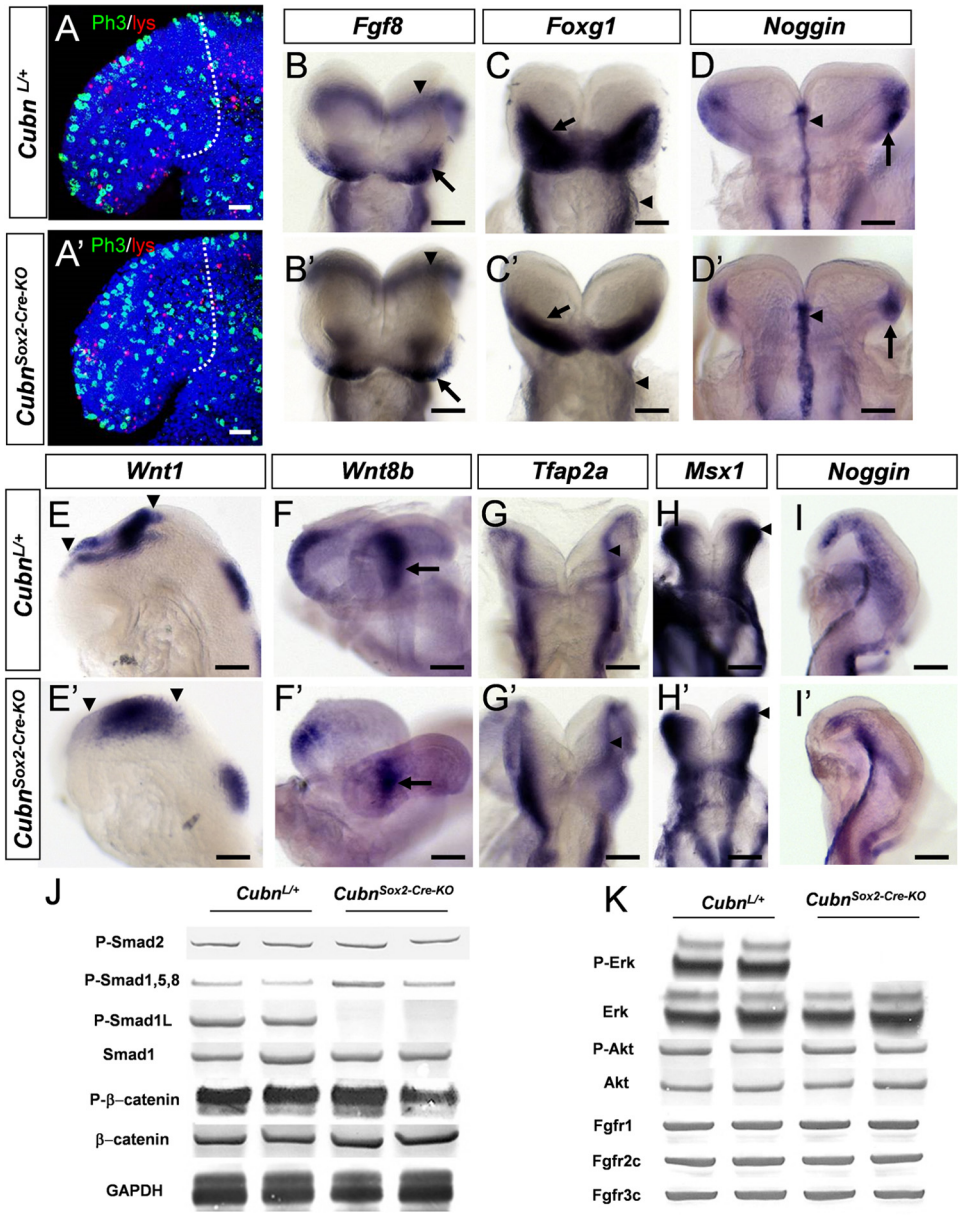

FIGURE 4. **Normal forebrain regionalization and impaired MAPK signaling in E8.75 *Cubn*$^{Sox2\text{-}Cre\text{-}KO}$ mutant heads.** *A* and *A′*, representative lateral views of E8.75 control and *Cubn*$^{Sox2\text{-}Cre\text{-}KO}$ embryos stained with Lysotracker (in *red*) and anti-phospho-histone H3 (in *green*). *Dotted lines* demarcate the forebrain region in confocal sections of an 8-ss control (*A*) and mutant (*A′*) embryo. Nuclei colored by Hoechst are shown in *blue*. *B–I*, representative whole-mount mRNA staining of control (*B–I*) and mutant (*B′–I′*) embryos at E8.75. *B* and *B′*, normal *Fg8* expression in the ANR (*arrow*) and the isthmus (*arrowhead*). *C* and *C′*, *Foxg1* is expressed in the anterior neural plate (*arrow*); it is reduced in the mutant pharyngeal region (*arrowhead*). *D* and *D′*, *Noggin* is normally detected in the rostral axial mesendoderm (*arrowhead*) and the rostrolateral ectoderm (*arrow*). *E–F′*, normal expression of *Wnt1* in the developing midbrain (*arrowheads* in *E* and *E′*) and of *Wnt8b* in the developing caudal forebrain (*arrow* in *F* and *F′*). *G–H′*, dorsal views of control and mutant embryos at the level of the prospective midbrain (*arrowhead*) and hindbrain showing *Tfap2a* normally expressed in the dorsal neural folds (*G* and *G′*) and *Msx1* in the dorsal neural folds and cephalic mesenchyme (*H* and *H′*). *I* and *I′*, *Noggin* is similarly found in a lateral strip of cells between the rostral-most cephalic mesenchyme and the border of the rhombencephalon (r2–r3). Frontal views (*B–D′*); lateral views with the anterior to the left (*E–F′* and *I* and *I′*). *J*, immunoblot analysis of cephalic extracts for phospho-Smad2, phospho-Smad1/5/8, phospho-Smad1Linker, total Smad1, phospho-β-catenin, and β-catenin. GAPDH is used as loading control. *K*, phospho-ERK1/2 is decreased, and phospho-Akt is maintained. The levels of endogenous total ERK and Akt are shown for comparison. The levels of FgfR1, FgfR2c, and Fgfr3c are normal in the mutants. *Scale bars*, *A*, 30 μm; *B–D*, 100 μm; *E*, *H*, and *I*, 6 μm; *F* and *G*, 40 μm.

were not co-immunoprecipitated with Cubn. Similarly, neither Wnt1, Wnt8b, Wnt3, Bmp7, nor Noggin were detected in the immunoprecipitates (supplemental Fig. 6*A*).

Further SPR analysis showed that recombinant mouse Fgf8a and Fgf8b, the two biologically active Fgf8 isomorphs (44, 45), bound in a Ca^{2+}-dependent manner and with equally high affinity to a purified Cubn chip (Fig. 5*B*). The dissociation constant (K_d) was calculated to 20 nM, a value orders of magnitudes higher than those reported for binding of Fgf8b and Fgf8a to their established receptors (K_d values of ~126–492 and 1–2.5 mM, respectively) (45). The equally high affinity of Fgf8a, the shorter Fgf8 isoform, and Fgf8b for Cubn indicated that the binding site of Fgf8 to Cubn was localized in the common core of the Fgf8 isoforms. Binding of Fgf8a or Fgf8b to Cubn was neither enhanced nor inhibited by recombinant FgfR1 or FgfR2 (supplemental Fig. 6*B*) indicating the following: (i) that the

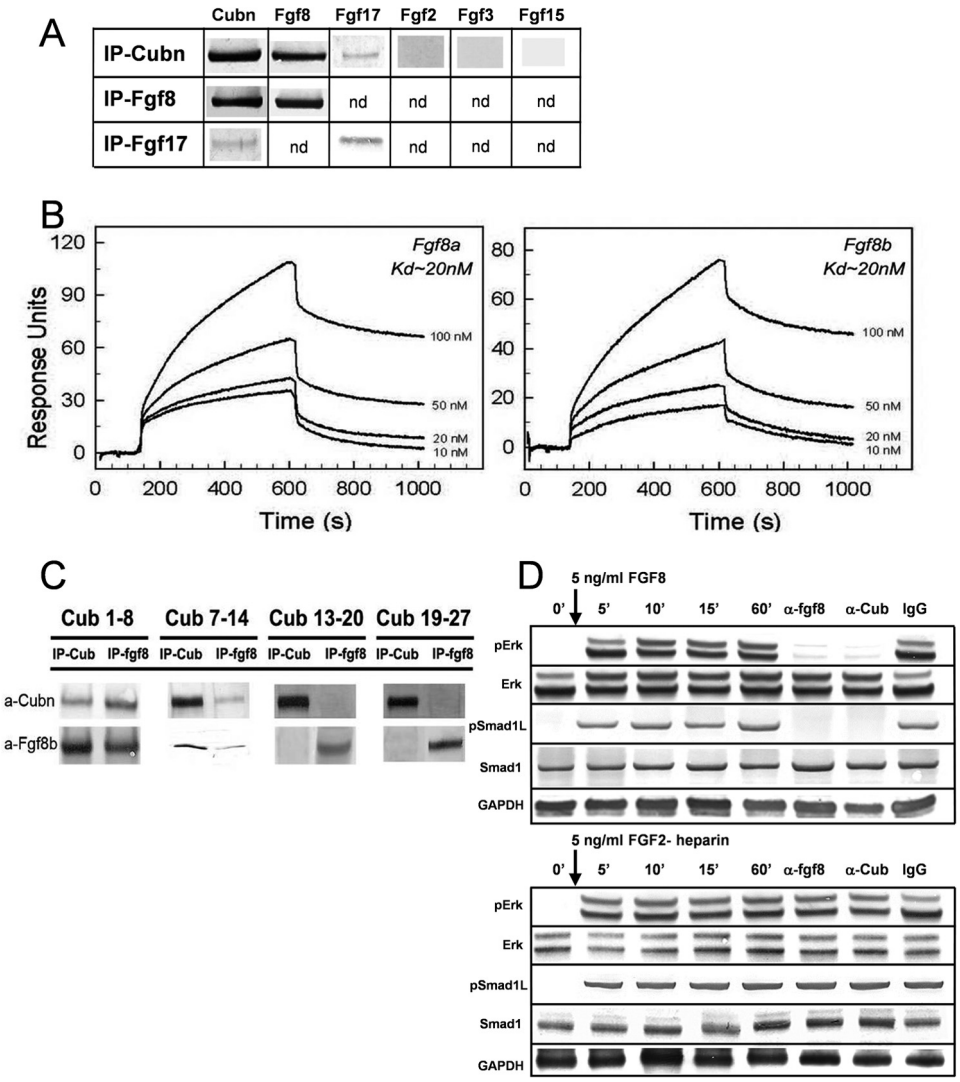

FIGURE 5. **Cubn binds Fgf8 with high affinity and contributes to Fgf8 signaling *in vitro*.** *A,* co-immunoprecipitation (*IP*) of Fgf8 and the structurally similar Fgf17 with Cubn; Fgf2, Fgf3, or Fgf15 do not interact with Cubn. *B,* SPR analysis on immobilized Cubn. Fgf8a and Fgf8b bind with equally high affinity to Cubn. *C,* immunoprecipitation of the "mini-proteins" CUB1–8, -7–14, -13–20, and -19–27 preincubated with recombinant Fgf8b without heparin and with anti-Fgf8b and anti-Cubn antibodies. Fgf8b preferentially co-immunoprecipitates with CUB1–8 and CUB7–14. *D,* incubation of serum-deprived BN/MSV cells with either 5 ng/ml of recombinant Fgf8b without heparin or recombinant Fgf2-heparin results in similar phosphorylation of ERK1/2 and Smad1Linker. Anti-Cubn antibodies or anti-Fgf8b antibodies block the phosphorylation of ERK1/2 and Smad1Linker specifically in Fgf8b-treated cells. Control IgG has no effect. Endogenous Smad1 and ERK1/2 levels are shown for comparison, and GAPDH is used as loading control.

binding sites of Fgf8 to Cubn and to FgfRs are distinct; (ii) that FgfRs and Cubn do not directly interact, and (iii) that Cubn, Fgf8, and FgfRs do not form ternary complexes. Fgf8b did not bind to a control chip with the molecular partner of Cubn, Lrp2 (14). A very low affinity in the micromolar range was recorded for recombinant mouse Bmp7, which interacted also with the control Lrp2 chip.

To further characterize the interaction between Cubn and Fgf8, we incubated Fgf8b with overlapping recombinant Cubn constructs encoding the CUB domains 1–8, 7–14, 13–20, and 19–27 (20). Immunoprecipitation with Sepharose-bound anti-Cubn and anti-Fgf8b antibodies identified CUB domains 1–8 and 7–14 as the ones to be most likely involved in the interaction with Fgf8b (Fig. 5*C*).

To distinguish between FgfR-mediated and Cubn-assisted internalization of Fgf8 and to verify that internalization of Cubn-bound Fgf8 results in the phosphorylation of the ERK1/2 and Smad1 linker, we incubated Cubn expressing BN/MSV cells (46) with recombinant Fgf8b for 5 min without the addition of heparin, a component required for Fgf ligand binding to FgfRs (47). As a control of Cubn-independent FgfR activation, we in parallel incubated BN/MSV cells with recombinant heparin-bound Fgf2. Phosphorylation of ERK1/2 and Smad1 linker was first detectable 5 min after addition of Fgf8b or Fgf2-heparin and was sustained over the time of the experiment, *i.e.* 60 min (Fig. 5*D*). In Fg8b-treated cells, endocytosis blocking anti-Cubn antibodies (18) or bioactivity neutralizing anti-Fgf8b antibodies (100 μg/ml) prevented the phosphorylation of both ERK1/2 and Smad1 linker (Ser-206), whereas control IgG had no effect (Fig. 5*D*). In contrast, in Fgf2 heparin-treated cells, the phosphorylation of neither ERK1/2 nor Smad1 linker was modified by anti-Cubn antibodies. These results demonstrate that Fgf8 is a specific high affinity ligand of Cubn and that Cubn-assisted Fgf8 internalization results in Fgf8 signaling.

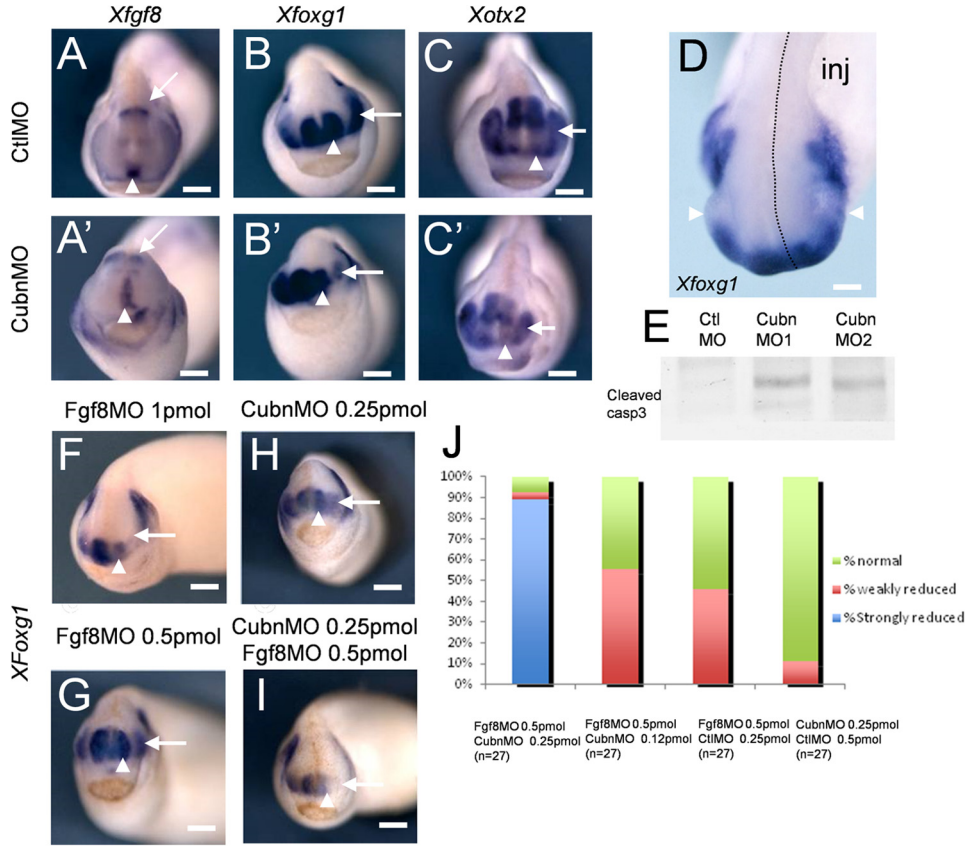

FIGURE 6. ***XCubn* and *XFgf8* are together necessary for normal head formation in the frog embryo.** *A–C′*, representative whole-mount mRNA staining of tailbud stage frog embryos unilaterally injected with control (*A–C*) and MoCubn (*A′–C′*) morpholinos. *A* and *A′*, *XFgf8* is expressed in the ANR (*arrowhead*) and the isthmus (*arrow*) of the MoCubn-treated embryos. *B* and *B′*, reduced *XFoxg1* expression domain in the telencephalon (*arrowhead*) and eye (*arrow*) after MoCubn injection. *C* and *C′*, reduced expression domain of *XOtx2* in the developing telencephalon (*arrowhead*), eye (*arrow*), and slightly in the midbrain of the MoCubn treated embryo. *D*, telencephalic and eye (*arrowhead*) hypoplasia and down-regulation of *XFoxg1* mRNA staining in the injected part of the embryo (*dotted line, inj*). *E*, increased levels of cleaved caspase-3 in cephalic extracts of MoCubn-treated embryos. *F*, telencephalic hypoplasia and down-regulation of *XFoxg1* in *MoFgf8*-injected embryos. *G* and *H*, low *MoFgf8* (0.5 pmol) or *MoCubn* (0.25 pmol) concentrations do not affect telencephalic development and *XFoxg1* expression. *I*, strong reduction of *XFoxg1* in embryos co-injected with *MoCubn* and *MoFgf8* at the same low concentrations. *J*, reduced or normal expression of *XFoxg1* after co-injection of MoCubn and MoFgf8 at the concentrations indicated. The number of embryos analyzed is indicated. *Scale bars*, *A–C*, and *F–I*, 250 μm; *D*, 75 μm.

We then wondered whether *Cubn* and *Fgf8* cooperate during head morphogenesis *in vivo* and whether *Cubn* expressed in the CNCCs is involved in the CNCC-*Fgf8* cross-talk, a process critical for the formation of the cephalic vesicles (33, 48, 49). We failed to obtain mouse mutants lacking both *Cubn* and *Fgf8* in the epiblast and to inactivate *Cubn* in the neural crest cells, including the rostral most CNCC population using mice expressing *Cre*-recombinase under the control of *Wnt1* cis-regulatory elements. We therefore continued our study using frog and chick embryos.

Synergistic Interplay between Cubn and Fgf8 during Head Formation—Quantitative RT-PCR analysis showed that *XCubn* mRNA was enriched in the anterior neural plate region of neurula stage frog embryos, and this was confirmed at the protein level (supplemental Fig. 7, *A* and *B*). We selectively depleted *Cubn* in the left side of the head by microinjecting translation-blocking antisense morpholino nucleotides into the left dorso-animal blastomere of 8-cell stage embryos (supplemental Fig. 7*C*). The expression of *XFgf8* in the ANR and the isthmus was maintained independently of the morpholino used (Fig. 6, *A* and *A′*). However, they both led to reduction of the expression domains of *XFoxg1* (Fig. 6, *B* and *B′*) and *XOtx2* (Fig. 6, *C* and *C′*) as well as to hypoplasia of the telencephalic and eye vesicles (Fig. 6*D* and supplemental Fig. 7*D*). Western blot analysis of treated embryos showed increased levels of activated caspase-3 (Fig. 6*E*) indicating that hypoplasia was accompanied by enhanced apoptosis.

Forebrain hypoplasia and reduced *XFoxg1* expression were as expected, also observed after depletion of *XFgf8* (Fig. 6*F*). We next identified concentrations of *XCubn* and *XFgf8* morpholinos, which did not modify telencephalic development and *XFoxg1* expression when injected individually (Fig. 6, *G* and *H*). Combined, these morpholinos induced severe telencephalic hypoplasia and complete down-regulation of *XFoxg1* in two independent experiments and in 24 out of 27 doubly injected embryos (Fig. 6, *I* and *J*, and supplemental Fig. 7*E*). These results support the idea that *XCubn* and *XFgf8* act synergistically during head morphogenesis.

Cubn Is Required for CNCC Survival and Head Formation—In the chick embryo, before CNCC migration, at the 5 ss, *Cubn* is detectable at low levels in the cephalic ectoderm (CE) flanking the ANR region and in the neural folds at the level of the prospective fore-, mid-, and rostral hindbrain, *i.e.* the presumptive CNCC (supplemental Fig. 8, *A* and *B*). After neural tube

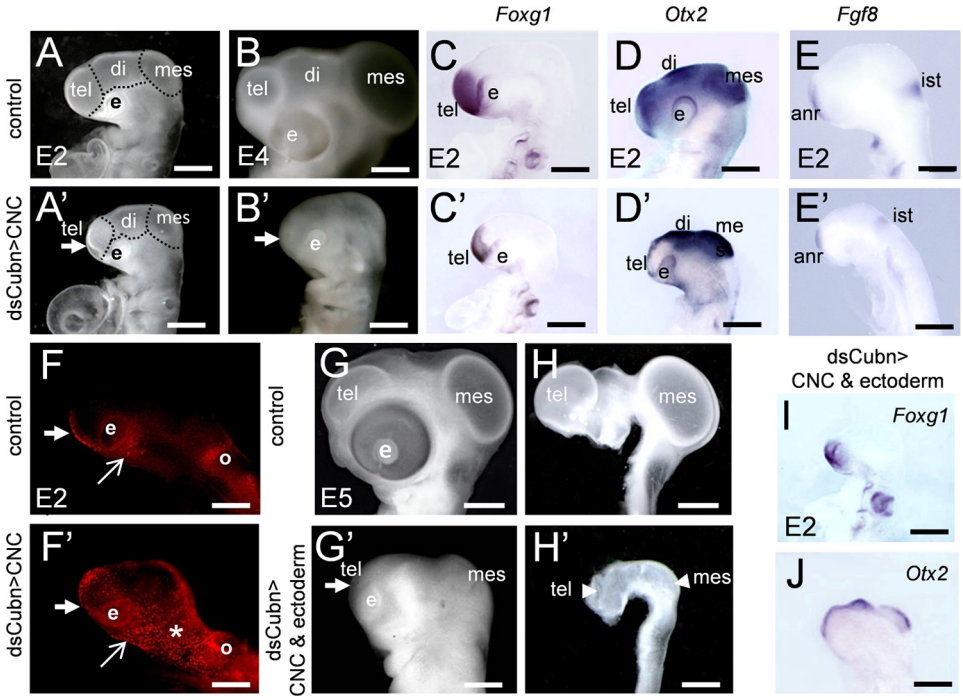

FIGURE 7. **Cubn expressed in the CNCC is critical for chick head formation.** *A–B′*, electroporation of *dsCubn* in the premigratory CNCC leads to severe cephalic reduction (*arrow* points to the telencephalon) at E2 (*A* and *A′*) and E4 (*B* and *B′*). *C–E′*, representative whole-mount mRNA staining for *Foxg1*, *Otx2*, and *Fgf8* in control (*C–E*) and *dsCubn*-treated (*C′–E′*) embryos. Silencing of *Cubn* in the CNCC leads to decreased *Foxg1* (*C* and *C′*) and *Otx2* (*D* and *D′*) expression domains in the telencephalon, whereas *Fgf8* (*E* and *E′*) remains expressed in the ANR. *F* and *F′*, LysoTracker staining at ~E1.5 shows enhanced cell death in the head at the level of the rostral forebrain (*thick arrow*), the lateral (*asterisk*), and the ventral cephalic mesenchyme (*arrow*) of a *dsCubn*-treated embryo. *G–H′*, silencing of *Cubn* in the premigratory CNCC and CE leads to severe cephalic hypoplasia at E5 (*G* and *G′*); the cephalic vesicles fail to expand normally (*H* and *H′*). *I* and *J*, representative whole-mount mRNA staining for *Foxg1* (*I*) and *Otx2* (*J*) after *Cubn* silencing in the CNCC and CE. Lateral views, anterior is to the left. *di*, diencephalons; *e*, eye; *ist*, isthmus; *mes*, mesencephalon; *o*, otic; *tel*, telencephalon. *Scale bars, A, A′, C–E′, I,* and *J,* 100 μm; *B* and *B′*, 600 μm; *G–H′*, 900 μm.

closure and CNCC migration, *Cubn* remains restricted to the prospective anterior CE, rostroventral forebrain, and post-migratory CNCC (supplemental Fig. 8, *C–E*).

We silenced endogenous *Cubn* specifically in the cephalic neural folds or in both the cephalic neural folds and the anterior CE by electroporating *dsCubn* mRNA at the 5 ss, before the onset of CNCC migration. Twenty four hours later, *i.e.* at the 25 ss, and independently of the experimental design used, head morphogenesis was severely affected (Fig. 7, *A–B′*, and *G–H′*). Although the neural tube remained closed, the fore- and midbrain vesicles failed to expand, and the head volume was reduced by 42% in the treated embryos compared with the controls ($n = 10$). Despite the reduction of the expression domains of *Foxg1* (Fig. 7, *C*, *C′*, and *I*) and *Otx2* (Fig. 7, *D*, *D′*, and *J*) silencing of *Cubn* did not affect fore- or midbrain patterning, and *Fgf8* was readily detected in the ANR and isthmus (Fig. 7, *E* and *E′*).

We noted that the decrease in head size correlated with extensive cell death, observed mainly in the cephalic mesenchyme a few hours after *Cubn* silencing, *i.e.* at the 18 ss (Fig. 7, *F* and *F′*). To verify that *Cubn* expressed in the migratory CNCCs functions, either directly or indirectly to regulate cell survival, we overexpressed the survival factor *Noggin*, a CNCC-produced factor known to potentiate Fgf8 signaling by counteracting Bmp activity (22), in the *Cubn*-depleted CNCCs. Overexpression of RCAS-*Noggin* in the CNCCs rescued the morphological defects and allowed normal fore- and midbrain formation (Fig. 8, *A–A″*). These results indicate that *Cubn* expressed in the migratory CNCCs is necessary for cell survival most likely by regulating CNCC response to Fgf8 signals.

We next sought to identify the FgfRs involved in Fgf8 signal reception in the CNCCs and document the potential interactions between *Cubn* and *FgfRs in vivo*. *FgfR3*, *FgfR1*, and to a lesser extent *FgfR2* are expressed in the presumptive CNCCs and CE (50, 51) in a pattern similar to *Cubn*. Silencing of *FgfR3* at the 5 ss resulted in fore-, midbrain, and facial hypoplasia (Fig. 8, *B–C′*), although less severe than the ones seen in *dsCubn*-treated embryos (Fig. 7, *G–H′*), whereas electroporation with *dsFgfR1* or *dsFgfR2* did not affect head development (Fig. 8, *B″–C‴*). We therefore further focused on *FgfR3* and *Cubn* and depleted the CE and cephalic neural folds from both *Cubn* and *FgfR3.* This double *Cubn-FgfR3* silencing aggravated the individual phenotypes and led to cephalic aplasia (Fig. 8, *D–D″*) and lethality the day following the electroporation. This set of results shows that in the chick embryo *FgfR3* is critical for Fgf, including Fgf8, signaling in the head and provides evidence that *Cubn* acts synergistically with *FgfR3* in the CNCC and CE to convey signals for anterior cell survival and head morphogenesis (Fig. 8*E*).

DISCUSSION

In this study, we identify a novel developmental role of embryonic *Cubn* in the vertebrate head. Ablation of embryonic *Cubn* leads to head hypoplasia that correlates with increased anterior cell death, abnormal distribution of

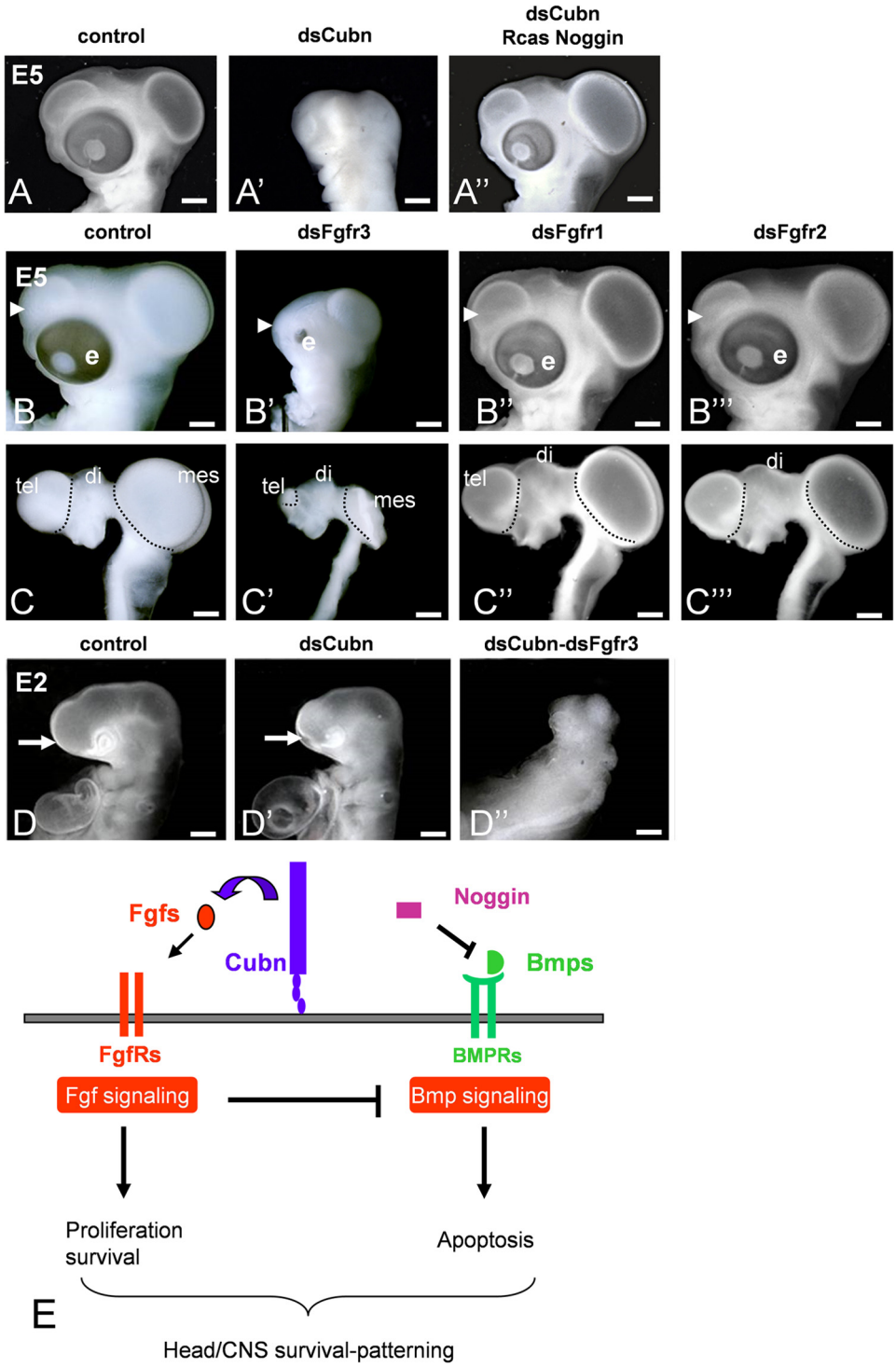

FIGURE 8. **Cubn promotes Fgf signaling in the chick CNCC and CE together with *FgfR3*.** *A–A″*, overexpression of *Noggin* in the CNCC of *dsCubn*-treated embryos restores head morphology. *B–C‴*, representative gross (*B–B‴*) and brain (*C–C‴*) morphology of E5 embryos electroporated in the CNCC and CE with *dsControl* (*B* and *C*), *dsFgfR3* (*B′* and *C′*), *dsFgfR1* (*B″* and *C″*), and *dsFgR2* (*B‴* and *C‴*). Cephalic hypoplasia is observed exclusively in *dsFgfR3*-treated embryos (*arrowhead* points to the telencephalon). *D–D″*, extremely severe head hypoplasia in double *dsCubn-dsFgfR3* electroporated embryos at E2 (*D″*) compared with *dsCubn*-treated embryos of the same stage (*D′*). *E*, proposed Cubn-Fgf8 interaction in the CNCC and CE. Cubn expressed at the plasma membrane binds extracellular Fgf8, favors its endocytosis (assisted by Lrp2 and/or a yet unknown partner), and increases its availability for FgfRs within the cell. Cubn-dependent FgfR activation together with Bmp antagonism, here via Noggin, is necessary to counter Bmp activity and promote CNCC and CE survival. *Scale bars*, *A–C‴*, 900 μm; *D–D″*, 100 μm.

migratory CNCCs, and decreased expression of phosphorylated ERK, events that may be explained by deficient Fgf signaling. High affinity binding of Fgf8 to Cubn leading to ERK phosphorylation as well as synergistic function between *Cubn* and *Fgf8* in the anterior head and *Cubn* and *FgfR3* in the migratory CNCC and CE support our conclusion that Cubn may act as an extracellular modulator of Fgf8 signaling during head morphogenesis.

Cubn Expressed in the Cephalic Neural Crest Is Necessary for Head Morphogenesis but Not Patterning—During the early somitic stages, murine *Cubn* is expressed in the forebrain and the cephalic neural folds. After neural tube closure, *Cubn* remains detectable in the neuroepithelium and in the cephalic mesenchyme but is excluded from the cephalic ectoderm. Partial co-localization with Tfap2α indicates that Cubn is expressed in the migratory CNCCs. At later developmental stages *Cubn* is also expressed in various tissues of endodermal and mesodermal origin (7).

The epiblast-specific inactivation of *Cubn* resulting in efficient ablation of embryonic *Cubn* shows that *Cubn* is critical for head morphogenesis but does not allow the unambiguous identification of the embryonic tissues at the origin of the head defects. Several lines of evidence indicate however that mesodermal and endodermal development are normal in $Cubn^{Sox2\text{-}Cre\text{-}KO}$ mutants at least until E9.5 and that the cephalic hypoplasia is neither the consequence of a developmental arrest nor of a heart defect. (*a*) The induction and maintenance of the anterior and forebrain identity as evidenced by *Otx2*, *Hesx1*, *Six3,* and *Fgf8 in situ* hybridization are not modified in the mutants. (*b*) Somite and body axis formation and turning onset around the 8–10 somite stage occur normally. (*c*) At the same stage, the expression of *Bmp7* in the mutant embryonic heart region is normal. (*d*) A normal beating heart lying posterior/ventral to the head is seen until E9.5. (*e*) PECAM-1 immunocytochemistry, which is routinely used to detail embryonic vasculature, clearly detects well developed blood vessels at the level of the forebrain at E9.5. It is thus unlikely that a cardiovascular system failure or a delayed growth may explain the cephalic hypoplasia of the mutants.

Combined, the results obtained in the mouse, frog, and chick embryos show that the head hypoplasia is not due to defective patterning indicating that *Cubn* is not absolutely required for this process. In the mouse embryo, the lack of *Shh* and *Nkx2.1* specifically in the preoptic area is the only forebrain defect at E9.25. This defect previously described in *Fgf8* hypomorphs (52) may be explained by deficient Fgf8 signal reception within the neuroepithelium of the $Cubn^{Sox2\text{-}Cre\text{-}KO}$ mutants and is unlikely to reflect a primary defect in Shh signaling. This is indicated by the normal expression of the Shh signaling readout *Gli1* (53), as well as the unmodified expression of *Shh* itself and *Six3* in the ventral forebrain of the mutants between E8.25 and E8.75.

To inactivate *Cubn* in the forebrain neuroepithelium or the cephalic neural crest selectively, we generated $Cubn^{Foxg1\text{-}Cre\text{-}KO}$ and $Cubn^{Wnt1\text{-}Cre\text{-}KO}$ mutants. We have been unsuccessful to efficiently delete *Cubn* in both cases. Most likely due to protein stability, Cubn was detectable in the forebrain of $Cubn^{Foxg1\text{-}Cre\text{-}KO}$ mutants until E10.5. Furthermore, *Cubn* remained detectable in the CNCC of the rostral most forebrain region of $Cubn^{Wnt1\text{-}Cre\text{-}KO}$ mutants. *XCubn* silencing in the anterior head of the frog embryo provided the first direct indication that *Cubn* was necessary for head morphogenesis. It is the use of the chick embryo that allowed us to clearly define that CNCC is the most important site of *Cubn* expression/function during head morphogenesis.

CNCC is considered as a signaling center critical for neural tube closure and normal cephalic vesicle formation (22, 33). In both mouse and chick, the cephalic neural crest has a double function; it responds to Fgf8 survival, proliferation, and migration signals and maintains Fgf8 expression and signaling from the ANR by secreting Bmp antagonists (31–33). Our results support the idea that Cubn is crucial for this cross-talk, in particular for the reception of the Fgf8 survival signals by the CNCCs. Indeed, enhanced cell death is observed in the cephalic mesenchyme but not the neuroepithelium of $Cubn^{Sox2\text{-}Cre\text{-}KO}$ mutant or *dsCubn*-treated embryos despite normal *Fgf8* expression and presumably normal Bmp antagonism. Thus *Cubn* expressed in the CNCCs is a novel, essential, and conserved modulator of head morphogenesis in the developing vertebrate head.

Cubn and Fgf8 Counteract Pro-apoptotic Bmp Activity—Fine-tuning of the equilibrium between Bmp, Wnt, and Fgf pro- and anti-apoptotic activities depends on the phosphorylation of the main Bmp effector Smad1 (40). Bmps promote C-terminal phosphorylation of Smad1/5/8, which is required for Bmp signaling (40). This process is identical in E8.75 wild-type and $Cubn^{Sox2\text{-}Cre\text{-}KO}$ mutant embryos indicating that the intensity of the pro-apoptotic Bmp signal is not modified and that retinoic acid activity, which suppresses Bmp activity by promoting degradation of C-terminal phosphorylated Smad1 (54), is normal. On the anti-apoptotic side, Fgf/MAPK and GSK3 mediate two sequential phosphorylations of the Smad1 linker region, which limit the duration of the Bmp signal (39, 55). In E8.75 $Cubn^{Sox2\text{-}Cre\text{-}KO}$ mutants, before any morphological abnormality can be seen, phosphorylation of Smad1 linker is undetectable indicating prolonged apoptotic activity. There is no evidence to link deficient Smad1 linker phosphorylation with deficient or increased Wnt activity because the expression levels of the Wnt targets β-catenin and phosphorylated β-catenin are normal. In contrast, the decreased levels of phosphorylated ERK1/2 in the $Cubn^{Sox2\text{-}Cre\text{-}KO}$ mutants suggest decreased activity of the Fgf/MAPK/ERK pathway, which is normally required to prime the Smad1 linker for a second phosphorylation by Wnt activity-regulated GSK3 (39). Direct evidence for the involvement of Cubn in the Fgf8/ERK1/2 pathway comes from *in vitro* studies of Cubn-expressing BN/MSV cells. In this model, the phosphorylation of ERK1/2 is similarly induced by Fgf8b or by heparin-bound Fgf2. In contrast, anti-Cubn or anti-Fgf8b antibodies block selectively the phosphorylation of ERK1/2 and the phosphorylation of Smad1 linker promoted by Fgf8b. We propose that absence of Smad1 phosphorylated in the linker region in the $Cubn^{Sox2\text{-}Cre\text{-}KO}$ mutants is due to a not fully efficient Fgf signaling and to a subsequently prolonged Bmp signal duration. The rescue of the phenotype of *dsCubn* mRNA-treated chick embryos by the overexpression of the Bmp antagonist Noggin supports this conclusion and shows that *Cubn* is absolutely necessary *in vivo* for an efficient Fgf-Bmp cross-regulation.

Cubn, a Novel Fgf8 Receptor and FgfRs Cooperate for Anterior Head Survival—There is no evidence supporting a direct interaction between Cubn and members of the Wnt or Bmp path-

ways involved in anterior cell survival. Our results show that Cubn is a novel and specific receptor for Fgf8. Joint silencing of *Cubn* and *Fgf8* in the early frog embryonic head aggravates the individual effects, and double *Cubn* and *FgfR3* downregulation in the chick CNCC and CE results in almost complete head truncation and embryonic death clearly indicating the interplay between *Cubn*, *Fgf8,* and *FgfRs* for anterior cell survival.

How this cooperation occurs at the cell level is not known. The subcellular distribution of FgfRs *in vivo* has not been reported extensively in the developing brain, but cell surface availability may be low (42). Gutin *et al.* (56) postulated the existence of extracellular and/or intracellular modulators that would impart specificity in Fgf responsiveness. In this context, Cubn, which binds to the core region of Fgf8 with high affinity, could "focus" members of the Fgf8 family to specific cell types, including the CNCC, and allow internalization of Fgf8 independently of FgfRs. Our data support this hypothesis; Cubn does not interact with FgfR1 or FgfR2 *in vitro* and presumably with other FgfR family members (57).

To behave as a distinct Fgf8 receptor, Cubn, which has no cytoplasmic domain, needs to interact with a transmembrane protein. Amn, a molecular partner of Cubn in the visceral endoderm and other absorptive epithelia, is hardly detectable in the neuroepithelium and not detectable in the CNCC. It is therefore unlikely that Amn is important for Cubn function in the anterior head. Supporting this hypothesis, Amn-deficient chimeras are viable (58). We propose that Lrp2, the other known endocytic partner of Cubn, expressed in the neuroepithelium and CNCC may at least partly facilitate endocytosis of Cubn-bound Fgf8. However, because the phenotype of the epiblast-specific *Lrp2* mutants is milder (15) than that of *Cubn* mutants, it is likely that Cubn interacts with additional yet not identified transmembrane proteins in the developing head.

Finally, polymorphisms in *CUBN* were proposed to be risk factors for neural tube closure defects (5, 6). We cannot exclude that this type of defects may be due to inadequate B12 levels in the mother or the fetus. However, neural tube closure defects are not associated with the selective vitamin B12 malabsorption Imerslund-Gräsbeck syndrome (23), and the maternal-to-fetal transport of vitamin B12 does not involve CUBN. Neural tube closure was not modified after selective *Cubn* ablation in the animal models and at the stages analyzed here. However, somite and body axis formation is severely perturbed in *Cubn* null mice (8). In view of our data, it is tempting to propose that the above polymorphisms may selectively modify the binding capacities of Cubn for Fgf8 family members during very early developmental stages affecting thereby Fgf8-responsive tissues involved in neural tube closure such as the mesoderm.

In conclusion, Cubn is a novel receptor for Fgf8 and most likely the Fgf8 subfamily members Fgf17 and Fgf18, necessary for efficient FgfR signaling and cell survival during early head morphogenesis at least in the mouse, frog, and chick embryos. We propose that Cubn may favor FgfR activation by increasing Fgf-ligand endocytosis/availability in all Cubn-expressing tissues.

Acknowledgments—We thank R. Le Bouffant and I. Buisson for quantitative RT-PCR studies; A. Brändli for XCubn plasmid; E. Lacy for anti-Amn antibody; S. Thomasseau and I. Anselme for technical assistance; A. Camus, F. Causeret, L. Bally-Cuif, U. Borelo, A. Pierani, and S. Schneider-Maunoury for helpful discussions and critical reading of the manuscript, and J. A. Sahel for constant support.

REFERENCES

1. Kozyraki, R., and Gofflot, F. (2007) Multiligand endocytosis and congenital defects: roles of cubilin, megalin, and amnionless. *Curr. Pharm. Des.* **13,** 3038–3046
2. Amsellem, S., Gburek, J., Hamard, G., Nielsen, R., Willnow, T. E., Devuyst, O., Nexo, E., Verroust, P. J., Christensen, E. I., and Kozyraki, R. (2010) Cubilin is essential for albumin reabsorption in the renal proximal tubule. *J. Am. Soc. Nephrol.* **21,** 1859–1867
3. Kozyraki, R., and Cases, O. (2013) Vitamin B12 absorption: Mammalian physiology and acquired and inherited disorders. *Biochimie* **95,** 1002–1007
4. Reznichenko, A., Snieder, H., van den Born, J., de Borst, M. H., Damman, J., van Dijk, M. C., van Goor, H., Hepkema, B. G., Hillebrands, J.-L., Leuvenink, H. G., Niesing, J., Bakker, S. J., Seelen, M., Navis, G., and REGaTTA (REnal GeneTics TrAnsplantation) Groningen Group (2012) CUBN as a novel locus for end-stage renal disease: insights from renal transplantation. *PLoS ONE* **7,** e36512
5. Franke, B., Vermeulen, S. H., Steegers-Theunissen, R. P., Coenen, M. J., Schijvenaars, M. M., Scheffer, H., den Heijer, M., and Blom, H. J. (2009) An association study of 45 folate-related genes in spina bifida: Involvement of cubilin (CUBN) and tRNA aspartic acid methyltransferase 1 (TRDMT1). *Birth Defects Res. Part A Clin. Mol. Teratol.* **85,** 216–226
6. Pangilinan, F., Molloy, A. M., Mills, J. L., Troendle, J. F., Parle-McDermott, A., Signore, C., O'Leary, V. B., Chines, P., Seay, J. M., Geiler-Samerotte, K., Mitchell, A., VanderMeer, J. E., Krebs, K. M., Sanchez, A., Cornman-Homonoff, J., Stone, N., Conley, M., Kirke, P. N., Shane, B., Scott, J. M., and Brody, L. C. (2012) Evaluation of common genetic variants in 82 candidate genes as risk factors for neural tube defects. *BMC Med. Genet.* **13,** 62
7. Assémat, E., Châtelet, F., Chandellier, J., Commo, F., Cases, O., Verroust, P., and Kozyraki, R. (2005) Overlapping expression patterns of the multiligand endocytic receptors cubilin and megalin in the CNS, sensory organs and developing epithelia of the rodent embryo. *Gene Expr. Patterns* **6,** 69–78
8. Smith, B. T., Mussell, J. C., Fleming, P. A., Barth, J. L., Spyropoulos, D. D., Cooley, M. A., Drake, C. J., and Argraves, W. S. (2006) Targeted disruption of cubilin reveals essential developmental roles in the structure and function of endoderm and in somite formation. *BMC Dev. Biol.* **6,** 30
9. Assémat, E., Vinot, S., Gofflot, F., Linsel-Nitschke, P., Illien, F., Châtelet, F., Verroust, P., Louvet-Vallée, S., Rinninger, F., and Kozyraki, R. (2005) Expression and role of cubilin in the internalization of nutrients during the peri-implantation development of the rodent embryo. *Biol. Reprod.* **72,** 1079–1086
10. Hammad, S. M., Stefansson, S., Twal, W. O., Drake, C. J., Fleming, P., Remaley, A., Brewer, H. B., Jr., and Argraves, W. S. (1999) Cubilin, the endocytic receptor for intrinsic factor-vitamin B_{12} complex, mediates high density lipoprotein holoparticle endocytosis. *Proc. Natl. Acad. Sci. U.S.A.* **96,** 10158–10163
11. Moestrup, S. K., Kozyraki, R., Kristiansen, M., Kaysen, J. H., Rasmussen, H. H., Brault, D., Pontillon, F., Goda, F. O., Christensen, E. I., Hammond, T. G., and Verroust, P. J. (1998) The intrinsic factor-vitamin B12 receptor and target of teratogenic antibodies is a megalin-binding peripheral membrane protein with homology to developmental proteins. *J. Biol. Chem.* **273,** 5235–5242
12. Barth, J. L., and Argraves, W. S. (2001) Cubilin and megalin: partners in lipoprotein and vitamin metabolism. *Trends Cardiovasc. Med.* **11,** 26–31
13. Fyfe, J. C., Madsen, M., Højrup, P., Christensen, E. I., Tanner, S. M., de la Chapelle, A., He, Q., and Moestrup, S. K. (2004) The functional cobalamin

(vitamin B12)-intrinsic factor receptor is a novel complex of cubilin and amnionless. *Blood* **103,** 1573–1579
14. Christ, A., Christa, A., Kur, E., Lioubinski, O., Bachmann, S., Willnow, T. E., and Hammes, A. (2012) LRP2 is an auxiliary SHH receptor required to condition the forebrain ventral midline for inductive signals. *Dev. Cell* **22,** 268–278
15. Spoelgen, R., Hammes, A., Anzenberger, U., Zechner, D., Andersen, O. M., Jerchow, B., and Willnow, T. E. (2005) LRP2/megalin is required for patterning of the ventral telencephalon. *Development* **132,** 405–414
16. Kozyraki, R., Fyfe, J., Verroust, P. J., Jacobsen, C., Dautry-Varsat, A., Gburek, J., Willnow, T. E., Christensen, E. I., and Moestrup, S. K. (2001) Megalin-dependent cubilin-mediated endocytosis is a major pathway for the apical uptake of transferrin in polarized epithelia. *Proc. Natl. Acad. Sci. U.S.A.* **98,** 12491–12496
17. Zucker, R. M., Hunter, S., and Rogers, J. M. (1998) Confocal laser scanning microscopy of apoptosis in organogenesis-stage mouse embryos. *Cytometry* **33,** 348–354
18. Le Panse, S., Galceran, M., Pontillon, F., Lelongt, B., van de Putte, M., Ronco, P. M., and Verroust, P. J. (1995) Immunofunctional properties of a yolk sac epithelial cell line expressing two proteins gp280 and gp330 of the intermicrovillar area of proximal tubule cells: inhibition of endocytosis by the specific antibodies. *Eur. J. Cell Biol.* **67,** 120–129
19. Colas, A., Cartry, J., Buisson, I., Umbhauer, M., Smith, J. C., and Riou, J.-F. (2008) Mix. 1/2-dependent control of FGF availability during gastrulation is essential for pronephros development in *Xenopus*. *Dev. Biol.* **320,** 351–365
20. Kristiansen, M., Kozyraki, R., Jacobsen, C., Nexø, E., Verroust, P. J., and Moestrup, S. K. (1999) Molecular dissection of the intrinsic factor-vitamin B12 receptor, cubilin, discloses regions important for membrane association and ligand binding. *J. Biol. Chem.* **274,** 20540–20544
21. Nykjaer, A., Lee, R., Teng, K. K., Jansen, P., Madsen, P., Nielsen, M. S., Jacobsen, C., Kliemannel, M., Schwarz, E., Willnow, T. E., Hempstead, B. L., and Petersen, C. M. (2004) Sortilin is essential for proNGF-induced neuronal cell death. *Nature* **427,** 843–848
22. Creuzet, S. E. (2009) Regulation of pre-otic brain development by the cephalic neural crest. *Proc. Natl. Acad. Sci. U.S.A.* **106,** 15774–15779
23. Gräsbeck, R. (2006) Imerslund-Gräsbeck syndrome (selective vitamin B_{12} malabsorption with proteinuria). *Orphanet J. Rare Dis.* **1,** 17
24. Hayashi, S., Lewis, P., Pevny, L., and McMahon, A. P. (2002) Efficient gene modulation in mouse epiblast using a Sox2Cre transgenic mouse strain. *Gene Expr. Patterns* **2,** 93–97
25. Paek, H., Gutin, G., and Hébert, J. M. (2009) FGF signaling is strictly required to maintain early telencephalic precursor cell survival. *Development* **136,** 2457–2465
26. Anderson, R. M., Stottmann, R. W., Choi, M., and Klingensmith, J. (2006) Endogenous bone morphogenetic protein antagonists regulate mammalian neural crest generation and survival. *Dev. Dyn.* **235,** 2507–2520
27. Ohkubo, Y., Chiang, C., and Rubenstein, J. L. (2002) Coordinate regulation and synergistic actions of BMP4, SHH, and FGF8 in the rostral prosencephalon regulate morphogenesis of the telencephalic and optic vesicles. *Neuroscience* **111,** 1–17
28. Mason, I. (2007) Initiation to end point: the multiple roles of fibroblast growth factors in neural development. *Nat. Rev. Neurosci.* **8,** 583–596
29. Geng, X., and Oliver, G. (2009) Pathogenesis of holoprosencephaly. *J. Clin. Invest.* **119,** 1403–1413
30. Hébert, J. M., and Fishell, G. (2008) The genetics of early telencephalon patterning: some assembly required. *Nat. Rev. Neurosci.* **9,** 678–685
31. Hoch, R. V., Rubenstein, J. L., and Pleasure, S. (2009) Genes and signaling events that establish regional patterning of the mammalian forebrain. *Semin. Cell Dev. Biol.* **20,** 378–386
32. Klingensmith, J., Matsui, M., Yang, Y.-P., and Anderson, R. M. (2010) Roles of bone morphogenetic protein signaling and its antagonism in holoprosencephaly. *Am. J. Med. Genet. C Semin. Med. Genet.* **154C,** 43–51
33. Le Douarin, N. M., Couly, G., and Creuzet, S. E. (2012) The neural crest is a powerful regulator of pre-otic brain development. *Dev. Biol.* **366,** 74–82
34. Geng, X., Speirs, C., Lagutin, O., Inbal, A., Liu, W., Solnica-Krezel, L., Jeong, Y., Epstein, D. J., and Oliver, G. (2008) Haploinsufficiency of Six3 fails to activate Sonic hedgehog expression in the ventral forebrain and causes holoprosencephaly. *Dev. Cell* **15,** 236–247
35. Liu, W., Lagutin, O., Swindell, E., Jamrich, M., and Oliver, G. (2010) Neuroretina specification in mouse embryos requires Six3-mediated suppression of Wnt8b in the anterior neural plate. *J. Clin. Invest.* **120,** 3568–3577
36. Itasaki, N., and Hoppler, S. (2010) Cross-talk between Wnt and bone morphogenic protein signaling: a turbulent relationship. *Dev. Dyn.* **239,** 16–33
37. Eswarakumar, V. P., Lax, I., and Schlessinger, J. (2005) Cellular signaling by fibroblast growth factor receptors. *Cytokine Growth Factor Rev.* **16,** 139–149
38. Turner, N., and Grose, R. (2010) Fibroblast growth factor signalling: from development to cancer. *Nat. Rev. Cancer* **10,** 116–129
39. Sapkota, G., Alarcón, C., Spagnoli, F. M., Brivanlou, A. H., and Massagué, J. (2007) Balancing BMP signaling through integrated inputs into the Smad1 linker. *Mol. Cell* **25,** 441–454
40. Eivers, E., Demagny, H., and De Robertis, E. M. (2009) Integration of BMP and Wnt signaling via vertebrate Smad1/5/8 and *Drosophila* Mad. *Cytokine Growth Factor Rev.* **20,** 357–365
41. Shinya, M., Koshida, S., Sawada, A., Kuroiwa, A., and Takeda, H. (2001) Fgf signalling through MAPK cascade is required for development of the subpallial telencephalon in zebrafish embryos. *Development* **128,** 4153–4164
42. Regad, T., Roth, M., Bredenkamp, N., Illing, N., and Papalopulu, N. (2007) The neural progenitor-specifying activity of FoxG1 is antagonistically regulated by CKI and FGF. *Nat. Cell Biol.* **9,** 531–540
43. Guillemot, F., and Zimmer, C. (2011) From cradle to grave: the multiple roles of fibroblast growth factors in neural development. *Neuron* **71,** 574–588
44. Guo, Q., Li, K., Sunmonu, N. A., and Li, J. Y. (2010) Fgf8b-containing spliceforms, but not Fgf8a, are essential for Fgf8 function during development of the midbrain and cerebellum. *Dev. Biol.* **338,** 183–192
45. Olsen, S. K., Li, J. Y., Bromleigh, C., Eliseenkova, A. V., Ibrahimi, O. A., Lao, Z., Zhang, F., Linhardt, R. J., Joyner, A. L., and Mohammadi, M. (2006) Structural basis by which alternative splicing modulates the organizer activity of FGF8 in the brain. *Genes Dev.* **20,** 185–198
46. Nykjaer, A., Fyfe, J. C., Kozyraki, R., Leheste, J. R., Jacobsen, C., Nielsen, M. S., Verroust, P. J., Aminoff, M., de la Chapelle, A., Moestrup, S. K., Ray, R., Gliemann, J., Willnow, T. E., and Christensen, E. I. (2001) Cubilin dysfunction causes abnormal metabolism of the steroid hormone 25(OH) vitamin D_3. *Proc. Natl. Acad. Sci. U.S.A.* **98,** 13895–13900
47. Mohammadi, M., Olsen, S. K., and Goetz, R. (2005) A protein canyon in the FGF-FGF receptor dimer selects from an à la carte menu of heparan sulfate motifs. *Curr. Opin. Struct. Biol.* **15,** 506–516
48. Creuzet, S. E., Martinez, S., and Le Douarin, N. M. (2006) The cephalic neural crest exerts a critical effect on forebrain and midbrain development. *Proc. Natl. Acad. Sci. U.S.A.* **103,** 14033–14038
49. Creuzet, S., Schuler, B., Couly, G., and Le Douarin, N. M. (2004) Reciprocal relationships between Fgf8 and neural crest cells in facial and forebrain development. *Proc. Natl. Acad. Sci. U.S.A.* **101,** 4843–4847
50. Lunn, J. S., Fishwick, K. J., Halley, P. A., and Storey, K. G. (2007) A spatial and temporal map of FGF/Erk1/2 activity and response repertoires in the early chick embryo. *Dev. Biol.* **302,** 536–552
51. Walshe, J., and Mason, I. (2000) Expression of FGFR1, FGFR2 and FGFR3 during early neural development in the chick embryo. *Mech. Dev.* **90,** 103–110
52. Storm, E. E., Garel, S., Borello, U., Hebert, J. M., Martinez, S., McConnell, S. K., Martin, G. R., and Rubenstein, J. L. (2006) Dose-dependent functions of Fgf8 in regulating telencephalic patterning centers. *Development* **133,** 1831–1844
53. Bai, C. B., Auerbach, W., Lee, J. S., Stephen, D., and Joyner, A. L. (2002) Gli2, but not Gli1, is required for initial Shh signaling and ectopic activation of the Shh pathway. *Development* **129,** 4753–4761
54. Sheng, N., Xie, Z., Wang, C., Bai, G., Zhang, K., Zhu, Q., Song, J., Guillemot, F., Chen, Y.-G., Lin, A., and Jing, N. (2010) Retinoic acid regulates bone morphogenic protein signal duration by promoting the degradation of phosphorylated Smad1. *Proc. Natl. Acad. Sci. U.S.A.* **107,** 18886–18891
55. Fuentealba, L. C., Eivers, E., Ikeda, A., Hurtado, C., Kuroda, H., Pera, E. M., and De Robertis, E. M. (2007) Integrating patterning signals: Wnt/GSK3

regulates the duration of the BMP/Smad1 signal. *Cell* **131,** 980–993
56. Gutin, G., Fernandes, M., Palazzolo, L., Paek, H., Yu, K., Ornitz, D. M., McConnell, S. K., and Hébert, J. M. (2006) FGF signalling generates ventral telencephalic cells independently of SHH. *Development* **133,** 2937–2946
57. Olsen, S. K., Ibrahimi, O. A., Raucci, A., Zhang, F., Eliseenkova, A. V., Yayon, A., Basilico, C., Linhardt, R. J., Schlessinger, J., and Mohammadi, M. (2004) Insights into the molecular basis for fibroblast growth factor receptor autoinhibition and ligand-binding promiscuity. *Proc. Natl. Acad. Sci. U.S.A.* **101,** 935–940
58. Tomihara-Newberger, C., Haub, O., Lee, H. G., Soares, V., Manova, K., and Lacy, E. (1998) The amn gene product is required in extraembryonic tissues for the generation of middle primitive streak derivatives. *Dev. Biol.* **204,** 34–54